THE HELIOGYRO

AN INTERPLANETARY FLYING MACHINE

By Richard H. MacNeal

March 1967

ARC-R-249

ASTRO
RESEARCH
CORPORATION

SANTA BARBARA, CALIFORNIA

THE HELIOGYRO

AN INTERPLANETARY FLYING MACHINE

By Richard H. MacNeal

March 1967

ARC-R-249

Prepared under Contract No. NAS7-427 by
ASTRO RESEARCH CORPORATION
Santa Barbara, California

for

NATIONAL AERONAUTICS AND SPACE ADMINISTRATION

THE HELIOGYRO, AN INTERPLANETARY FLYING MACHINE

By Richard H. MacNeal
Astro Research Corporation

ABSTRACT

A design concept is developed for a type of solar sail vehicle that employs long, narrow blades made from thin films and that operates in the manner of a helicopter rotor. The blades are unrolled from spools during deployment.

Three different versions of the heliogyro are described, including a small experimental two-blader, and two 100,000 pound gross-weight multi-bladed vehicles that are suitable for manned voyages to the inner planets.

Some of the engineering problems associated with structural design and operation are treated, including consideration of static blade deformations, control characteristics, deployment, and maneuvers in planetary orbit.

The performance of the heliogyro is discussed for a variety of missions including station keeping, station visiting, interplanetary travel and descent into planetary orbit. It is concluded that the heliogyro is superior to other systems employing chemical or electrical propulsion for many missions requiring a large total impulse. Engineering development appears to be technically feasible.

LIST OF SYMBOLS

A	surface area
a	acceleration
a_1	longitudinal component of cyclic pitch
b_1	lateral component of cyclic pitch
c	blade chord
E	Young's modulus
F_G	sun's gravitational force
F_Y	lateral control force
F_z	force parallel to spin axis
F_ψ	force in direction of orbital motion
f_r	coefficient of reflection
g_o	gravitational acceleration at surface of planet
h_i	orbital altitude above surface of planet
I	moment of inertia
I_{sp}	specific impulse
M_x	lateral control moment
M_y	longitudinal control moment

M_z moment about spin axis

$\dot{m}$ mass flow rate

m_v mass of vehicle

n_b number of blades

P power

p_a absorbed component of radiation pressure

p_d drag component of radiation pressure

p_ℓ lift component of radiation pressure

p_n component of pressure normal to surface

p_o total radiation pressure for normal incidence

p_r reflected component of radiation pressure

p_x chordwise component of pressure

R blade tip radius

R_1 initial pay-out radius

r distance from axis of rotation

$r_i = r_o + h_i$

r_o radius of planet

T thrust

T_o torque

t	time, thickness
t_e	time for planetary escape
t_2	time for gradual pay out
u	chordwise deflection
V	velocity of expelled particles
W	weight
w	deflection normal to blade
x	distance from mid-chord of blade
x_{cp}	chordwise location of center of pressure
x_t	chordwise location of tension axis
β	coning angle, $\frac{\partial w}{\partial r}$
β_o	coning angle at blade root
γ	incidence angle of illumination with respect to axis of spin
θ	incidence angle, pitch angle
θ_o	collective pitch
λ	lightness number = ratio of radiation force to sun's gravitational attraction
λ_u	wavelength of chordwise deformation
ρ	density of blade material

σ_o	spanwise stress at blade root
σ_r	spanwise stress
σ_x	chordwise stress
τ	rotation period
ψ	azimuth angle from reference
ψ_o	reference azimuth angle
Ω	rotational speed, (rad/unit time)

THE HELIOGYRO, AN INTERPLANETARY FLYING MACHINE

By Richard H. MacNeal
Astro Research Corporation

INTRODUCTION

The mechanical forces acting on a body in interplanetary space are, with the exception of gravitational attraction, very small compared to the forces experienced in our terrestrial environment. The largest of the "small" environmental forces in interplanetary space is a surface pressure due to the transfer of momentum from photons radiated by the sun. The average solar radiation pressure in the vicinity of the Earth is approximately equal to 0.9×10^{-4} dynes/cm^2 or, in English units, 0.1882×10^{-6} lb/ft^2 .

Since radiation pressure acts normal to a reflecting surface, in the manner of aerodynamic pressure in Newtonian flow, it can be used as a basis for the design of interplanetary flying machines. Such vehicles are known as solar sails and there is an extensive current technical literature (refs. 1-6) relating to their performance. Their wing loading is, of course, very low compared to conventional aircraft, but, given the fact that the acceleration imparted by radiation pressure acts continuously, vast distances can be traveled in time spans measured in months or years. The travel time on interplanetary missions is, in general, competitive with that of spacecraft employing chemical or ion propulsion.

The solar sail has an obvious and very large advantage over spacecraft that employ inertial reaction for propulsion, in that no fuel need be carried along. For long missions requiring several stages of acceleration or deceleration, the weight advantage can amount to two or more orders of magnitude (ref. 4).

In spite of the favorable performance characteristics of solar sails, none have been launched and none are included in current plans for space experiments. The reason for the lack of serious consideration afforded to the solar sail is related to

its size. A solar sail with acceptable performance requires about 1000 square feet of sail area per pound of useful load, so that even a small experimental spacecraft requires a very large sail. Although sufficiently light-weight sail materials are available, insufficient attention has been given to the practical problems involved in deploying and rigidizing such large areas. Until and unless credible solutions to these problems are found, the solar sail will not become a reality.

The subject of the present report is the development of a solar-sail design concept in which the problems associated with sail deployment and flight dynamics have practical solutions. The configurations that are described resemble helicopter rotors in appearance, (long narrow blades), in the manner by which they are rigidized (centrifugal force), and in the manner by which they are controlled (cyclic and collective blade pitch). The name that has been given to them is heliogyro, i.e., a rotating device that is propelled by the sun.

Emphasis will be placed on structural design and on the response to maneuver commands, including deployment. Aspects of solar sailing that are extensively treated in the technical literature, such as celestial navigation and the selection of sail materials, will be reviewed briefly.

REVIEW OF SOLAR SAIL TECHNOLOGY

Electromagnetic waves are partly reflected and partly absorbed at the surface of an object. The part that is reflected exerts a pressure

$$p_r = p_o \cdot f_r \cdot \cos^2\theta \qquad (1)$$

normal to the surface, where p_o is the total pressure for normal incidence, f_r is the coefficient of reflectivity and θ is the angle between the normal to the surface and the incident radiation. The part that is absorbed exerts a pressure

$$p_a = \frac{1}{2} \cdot p_o \left(1-f_r\right) \cos\theta \qquad (2)$$

in the direction of the incident radiation. The components of pressure may be combined to give the following expressions (ref. 6) for the components of pressure parallel to the illumination (drag) and perpendicular to the illumination (lift).

$$p_d = p_o \left(f_r \cdot \cos^3\theta + \frac{1}{2}\left(1 - f_r\right)\cos\theta \right) \tag{3}$$

$$p_\ell = p_o \left(f_r \cdot \cos^2\theta \cdot \sin\theta \right) \tag{4}$$

Since the metalized surface of a solar sail has a high coefficient of reflectivity, f_r is usually assumed to be unity in preliminary design studies.

For a flat sail in orbit around the sun, p_d acts directly away from the sun, and p_ℓ acts in the direction of orbital motion if the normal to the sail lies in the plane of the orbit. If the radiation force on the vehicle is small compared to the gravitational attraction of the sun, the eventual effect of p_d is to produce a small increase in the radius of the equilibrium orbit. The effect of p_ℓ on the other hand is to produce a continuous acceleration in the direction of motion, thereby increasing the angular momentum and permitting, in time, large changes (either positive or negative depending on the sign of θ) in the orbital radius.

The mechanics of the solar sail in orbit around the sun have been examined in a number of papers (refs. 2, 4, 6, and 7). The parameter most commonly used to characterize the performance of a solar sail is the lightness number, λ , defined as the ratio of the radiation force on the sail to the attractive force of the sun's gravitational field:

$$\lambda = \frac{p_o A}{F_G} \tag{5}$$

Since both p_o and F_G vary inversely as the square of the distance from the sun, the lightness number is independent of position within the solar system. The lightness number is related to the weight loading, W/A, by the formula

$$\lambda = .308 \times 10^{-3} \cdot \left(\frac{A}{W}\right) \tag{6}$$

where W is the weight in pounds and A is the area in square feet. The potential acceleration of the vehicle in the vicinity of the Earth due to radiation pressure is related to the lightness number by

$$a = \frac{p_o A}{W} = .611 \times 10^{-3} \lambda \tag{7}$$

where the acceleration, a, is expressed in Earth g's.

The travel time for voyages between planets has been computed as a function of the lightness number and of the variation of the sail angle, θ, during the voyage. If the radial component of pressure, p_d, is ignored (which is an accurate approximation only for very small values of λ) the shortest travel time is obtained for the largest value of p_ℓ, which occurs, from equation (4), when $\theta = 35° 15.9'$. When p_d is taken into account, the optimum sail angle varies along the trajectory. Figure 1 presents travel times for nearly optimal voyages from Earth to Mars (taken from refs. 6 & 7) as a function of lightness number. Two classes of voyages are considered. In fly-by missions, the objective is to leave a high earth orbit and to reach the vicinity of Mars in minimum time, without regard to the relative velocity between the spacecraft and Mars. In capture missions, the objective is to leave a high Earth orbit and to enter a high Mars orbit in minimum time. It is seen that the travel time for a fly-by mission is shorter and is more strongly dependent on lightness number than is the travel time for a capture mission. The vertical dashed line in Figure 1 indicates that, for a lightness number slightly below 0.08, a quantum jump to a value twice as large occurs in the travel time for capture missions. A lightness number equal to 0.08 is

therefore regarded as the practical lower limit for Mars capture missions.

Considerable attention has been directed to the question of practical materials for solar sail construction that will exhibit suitably low lightness numbers. It has been shown (ref. 2) that the maximum possible lightness number, resulting as a balance between film thickness and opacity, is around 5 and occurs for metal films that are too thin to be considered practical (about 500 A°). Aluminum sheets with thicknesses equal to 3000 A° that are deposited on plastic films that sublime in a space environment have been proposed, (ref. 1), but are considered to be well beyond the present state-of-art.

The most commonly considered material for solar sails is a Mylar sheet on which thin films of aluminum have been deposited. The reasons for the interest in Mylar is that it is the lightest continous film that is currently available in quantity, and that it has been successfully used for the Echo I balloon. Quarter mil aluminized Mylar sheets can be purchased in rolls 56" wide at a price under 2 cents per square foot. Samples of .05 mil Mylar have been produced.

Figure 2 shows the relationship between lightness number, payload weight fraction and sheet thickness for a Mylar sheet coated with 3000 A° of aluminum. For a given thickness of Mylar, a compromise between lightness number and payload weight fraction is made on the basis of overall performance considerations. Figure 2 indicates, for example, that 0.1 is a practical lightness number for standard 0.25 mil sheets and that 0.3 is a practical lightness number for .05 mil sheets.

The deleterious effects on solar sails of long exposures to a space environment have received attention. The hazards that have been considered (ref. 5) include temperature extremes, micrometeoroids, sputtering due to proton bombardment, and the deterioration of organic material due to irradiation by ultraviolet light.

Temperature is not considered to be an important problem as long as illumination angles near 90° are avoided. Sputtering of the thin aluminum coating due to solar protons was formerly considered to be a serious problem until recent experimental data (ref. 8) showed the erosion rate to be of the order of one angstrom

per year. Micrometeoroids are clearly not a significant threat to structural integrity since the proportion of the surface area punctured in one year's time is of the order of 10^{-5}. Damage to the Mylar sheet by ultraviolet radiation is effectively eliminated by the aluminum coating (ref. 9). The general conclusion to be drawn from the above studies of the effects of the space environment on solar sails is that no especially serious problems have been discovered.

An interesting fact about solar sails is that they are not suitable for low Earth orbits, due to the presence of aerodynamic effects. The dynamic pressure exceeds the solar radiation pressure for altitudes less than 600 KM. It has been assumed (ref. 6) that the minimum practical altitude for solar sail operation is about 800 KM (500 statute miles).

STRUCTURAL DESIGN CONCEPT

The structural design criteria that must be satisfied by a space vehicle employing solar radiation pressure for primary propulsion are the following.

a) Ability to deploy and rigidize an extremely large, light-weight, approximately flat surface.

b) Ability to execute maneuvers by changing the direction and/or magnitude of the solar radiation force.

c) Ability to be stored in and deployed from available launch vehicles.

The deployed surface area and total weight are determined by fundamental performance considerations and the properties of available materials as described in the preceding section. The overall dimensions of the stowed configuration are determined by the characteristics of existing boosters. The first set of decisions within the jurisdiction of the structural designer relates to the shape of the sail and the means used for deploying and rigidizing it.

There has been a tendency in the existing literature to assume, a priori, that the sail will be a solid circular disc,

which is the shape that minimizes the overall size, and which, presumably, also minimizes the weight required for rigidization. Unfortunately the solid circular disc presents formidable problems with regard to deployment since the sail must be folded in the stored configuration (assuming that the diameter of the disc exceeds the length of available booster payload compartments).

Folding can be avoided and the problems of deployment can be minimized by making the sail from a long rectangular strip, or strips, that are wound on spools in the stowed configuration. A potential disadvantage of this configuration is that the large overall dimension in the deployed state may lead to large structural weight, by virtue of the familiar square-cube law. It will be shown, however, that the square-cube law does not impose serious restrictions on the design of vehicles with as much as one hundred thousand pounds of gross weight.

The available methods for rigidizing the sail include the use of

a) Compression resistant structural members
b) Pneumatically stabilized structural members
c) Centrifugal force
d) Electrostatic force
e) Magnetostatic force

Methods a) and b) are particularly suitable for round solar sails. It is shown in reference 10, for example, that the weight of a rigidizing ring on the circumference of a sail of reasonable size is small compared to the weight of the sail. These methods are not suitable for long narrow sails.

Methods d) and e) have been studied in reference 11, where formulas and sample calculations are given for the tension in straight wires and circular discs due to electrostatic charge, and for the tension in a circular loop of current-carrying wire. Although electrical methods for rigidizing structures are interesting and have potential application in space, the voltages or currents needed to produce tensions of the magnitudes required in the present application are too large to be considered practical. A straight wire would, for example, require an electrostatic potential greater than a million volts to produce a tension of one pound in a long narrow sail.

Centrifugal force is an excellent, relatively simple method for rigidizing solar sails, and can be used for both round sails (refs. 2 and 5) and long narrow sails. Centrifugal force is probably the only practical method for rigidizing long narrow sails.

The main requirement in maneuvering a solar sail is the ability to change the orientation of the sail with respect to the illumination, which implies the ability to apply mechanical moments to the sail. The methods by which this may be done include

a) Inertial reaction from rocket motors
b) Shifting the center of gravity of the payload
c) Changing the angular momentum vector of the payload
d) Changing the distribution of radiation pressure on the sail.

Method a) has been avoided by solar sail enthusiasts for obvious reasons. Several schemes for applying methods b) and c) to round solar sails are described in reference 5. Method d) is particularly appealing for a vehicle employing two or more long narrow blades because the moment required to rotate a narrow blade about its lengthwise axis is very small.

The structural design concept developed in the present study employs long narrow blades that are rigidized by centrifugal force and which are rotated about their lengthwise axes to provide spin torque and precessional moments. The choice of long narrow blades was made primarily from consideration of the dimensional constraints imposed by launch vehicles and the resulting problems of deployment. Centrifugal force was selected as the means for rigidization because all other known methods are unsuitable for long narrow blades of the required size. Blade pitch was selected for the control system because of its mechanical simplicity and because it can provide all desired control responses (spin torque, precessional moment and modulation of the lift and drag forces).

In order to provide a quantitative basis for a discussion of the engineering problems associated with the design concept, a small number of specific vehicle configurations have been postulated. The first and simplest of these is shown in figures 3 and 4. It consists of a pair of blades that are connected to a payload capsule. Each blade is initially wound on a spool that is

connected by a pitch bearing and a pitch-change drive motor to the payload capsule. The unrolling of the blades from the spools is motor-controlled. The blade material is 1/4 mil Mylar with 1500A° of aluminum deposited on each side. Technical characteristics of the vehicle are summarized in Table I.

Engineering design begins with a consideration of the relationship between weight, performance and size of the vehicle. Figures 1 and 2 show that, for the selected sail material (1/4 mil aluminized Mylar), a reasonable compromise between performance and weight is obtained with a lightness number equal to 0.1 . If it is assumed (arbitrarily) that the non-sail weight is 200 lbs, figure 2 gives for the gross weight

$$W = \frac{200}{.364} = 550 \text{ lbs} \tag{8}$$

The deployed sail area as obtained from equation (6), is

$$A = \frac{W \cdot \lambda}{.308 \times 10^{-3}} = 180{,}000 \text{ ft}^2 \tag{9}$$

If the blade chord is chosen to be 4.84 ft, which is a commercially available width, the blade radius (semi-span) is:

$$R = \frac{A}{2c} = \frac{180{,}000}{2 \times 4.84} = 18{,}600 \text{ ft} \tag{10}$$

The size, shape and general performance characteristics of the vehicle have now been established. It remains to determine the rotational speed, the stress distribution, the maneuvering capability and the deployment sequence. These matters require analysis of the mechanics of a slender flexible blade subjected to centrifugal force and photon pressure, and they are treated in the next several sections of the report.

STATIC BLADE DEFORMATION

We are concerned with blade deformations of three types: vertical (or flapwise) deflection, in-plane (or chordwise) deflection, and twist. Although coupling between the different types of deformation should not be ignored, it is a great deal easier and at least instructive to do so.

Centrifugal force is the main stiffening agent in the present application for all three types of deformation. Consider a point (r, x) on the surface of a flat blade as shown in figure 5. The steady components of centrifugal force density are

$$f_r = \rho\Omega^2 r \tag{11}$$

$$f_x = \rho\Omega^2 x \tag{12}$$

The resulting membrane tensile stresses in a uniform rectangular blade are

$$\sigma_r = \int_r^R \rho\Omega^2 r\,dr = \frac{1}{2}\cdot\rho\Omega^2 (R^2 - r^2) \tag{13}$$

$$\sigma_x = \int_x^{c/2} \rho\Omega^2 x\,dx = \frac{1}{2}\cdot\rho\Omega^2 \left(\left(\frac{c}{2}\right)^2 - x^2 \right) \tag{14}$$

If the blade is considered to be a tensioned membrane, the differential equation describing small motions normal to its surface is

$$\frac{\partial}{\partial r}\left(\sigma_r \frac{\partial w}{\partial r}\right) + \frac{\partial}{\partial x}\left(\sigma_x \frac{\partial w}{\partial x}\right) + \frac{p_n}{t} = 0 \tag{15}$$

where p_n is the pressure normal to the surface and t is the

thickness of the blade.

For vertical deflection that is uncoupled to twist, $\frac{\partial w}{\partial x} = 0$, and equation (15) may be integrated to produce an expression for the local coning angle,

$$\beta = \frac{\partial w}{\partial r} = \frac{1}{\sigma_r} \int_r^R \frac{p_n}{t} \cdot dr = \frac{2p_n}{t\rho\Omega^2 (R + r)} \tag{16}$$

where the second form is appropriate for a uniformly loaded rectangular blade. Equation (16) shows that the coning angle at the root, β_o , is twice as large as the coning angle at the tip. Lack of straightness in the deflected shape produces mechanical coupling between chordwise deformation and twist which may be undesirable. A uniform coning angle can be achieved by tapering the blade chord and mass distribution along the span, as explained in ref. 12.

A relationship between coning angle and the axial stress at the blade root is obtained by noting that the axial stress at $r = 0$ is

$$\sigma_o = \frac{1}{2} \cdot \rho (\Omega R)^2 \tag{17}$$

so that

$$\beta_o = \frac{p_n R}{\sigma_o t} \tag{18}$$

As an example, consider the two-bladed vehicle described in the preceding section and let the stress at the blade root be 1000 psi. The normal pressure, p_n , is equal to the solar radiation pressure, p_o , minus the inertial reaction of the sail. Thus

$$p_n = \frac{\text{non-sail weight}}{\text{gross weight}} \times p_o = .364 \times .1882 \times 10^{-6}$$

$$= .0685 \times 10^{-6} \text{ lb/ft}^2$$

and, substituting into equation (18),

$$\beta_o = \frac{.0685 \times 10^{-6}}{(1000 \times 144)} \times \frac{(18600 \times 12)}{(.00025)} = .000425 \text{ radians}$$

Large coning angles should be avoided for a number of reasons. One reason, which applies only to very large angles, is that the thrust due to solar illumination parallel to the axis of rotation decreases as $\cos^3\beta$. Another reason is that, if the direction of illumination is not parallel to the axis of rotation, coning produces a steady processional torque on the vehicle. This effect is examined in the next section. A third reason, already noted, is that lack of straightness in the deflected shape produces mechanical coupling between chordwise deformation and twist. The vertical deflection obtained by integrating equation (16) is plotted in figure 6 and compared with a straight line drawn through the 75% span point. The maximum deviation is approximately equal to 5% of the vertical deflection at the tip. Thus for the example vehicle

$$\delta = .05\beta_o R = .05 \times .000425 \times 16,600 = .395 \text{ ft}$$

which is small compared to the blade chord.

Equation (18) shows that the coning angle is proportional to blade radius so that the effects of coning become more important as size is increased. Two other operational characteristics that depend on size are the rotational period and the centripetal acceleration at the blade tip. Formulas for these quantities are

$$\tau = 2\pi R\sqrt{\frac{\rho}{2\sigma_o}} \qquad (19)$$

and

$$g_{tip} = \frac{2\sigma_o}{\rho R} \tag{20}$$

Equations (18), (19) and (20) are plotted in figure 7 for a ¼ mil Mylar blade with 1000 psi root stress.

For operation near the surface of the Earth the rotational period should be small compared to the orbital period in order to minimize the effects of perturbing forces produced by gravity gradient. Assume that the minimum orbital period is 100 minutes and that the rotational period should be less than 20% of the orbital period. Figure 7 shows that this criterion is not satisfied for blade radii greater than 60,000 ft unless the root stress is increased above 1000 psi.

Centripetal acceleration can be used in manned vehicles to provide an artificial gravitational field for the occupants. Figure 7 shows that the tip acceleration falls below 0.1 g for radii greater than 35,000 ft. A larger acceleration can be obtained at the cost of higher stresses.

Turning now to a consideration of the effects of twist, let $w = \theta \cdot x$ in equation (15). Multiplication of both sides by x and integration over the chord then produces the following differential equation for θ .

$$\frac{\partial}{\partial r}\left(I\sigma_r \cdot \frac{\partial \theta}{\partial r}\right) - \rho\Omega^2 I \cdot \theta + t_\theta = 0 \tag{21}$$

where

$I = \frac{1}{12} \cdot c^3 t$ is the area moment of inertia of the cross section with respect to a vertical axis.

$$t_\theta = \int_{-c/2}^{+c/2} p_n x dx$$ is the moment of applied forces with respect to the mid-chord.

Equation (21) shows two interesting effects. The first is that the product $I\sigma_r$ replaces the familiar JG as the spanwise torsional stiffness. The second is that chordwise centrifugal force produces a restoring moment proportional to pitch angle. If the blade is oscillated in pitch at the rate of one cycle per revolution, the restoring moment will just exactly cancel the inertia moment.

A primary requirement is that it be possible to pitch the entire blade by imposing a steady pitch angle at the root end. The solution to equation (21) for a uniform rectangular blade with $t_\theta = 0$ is shown in figure 8.

The solution does not depend on any of the blade parameters (I, Ω, ρ, σ_r or c/R). The pitch angle at the tip is equal to 36.4% of the imposed pitch angle at the root.

The torque required to pitch the blade is

$$T_o = I\sigma_o \cdot \left.\frac{\partial\theta}{\partial r}\right|_{r=0} = 1.208\left(I\sigma_o\right)\cdot\frac{\theta_o}{R} \qquad (22)$$

For the example vehicle, neglecting the aluminum coatings

$$\sigma_o = 1000 \text{ psi}$$

$$I = \frac{1}{12}\cdot c^3 t = \frac{1}{12} \times (58)^3 \times .00025 = 4.07 \text{ in}^4$$

$$R = 18600 \times 12 = 223{,}000 \text{ in}$$

so that

$$T_o = \frac{1.208 \times 4.07 \times 1000}{223,000} \times \theta_o = .022\theta_o \text{ (in-lbs)}$$

which is very small.

Equation (21) may also be used to calculate the blade twist due to a chordwise offset between the center of pressure and the tension axis of the blade. The solution for a uniform offset is shown in figure 8 where the normalizing factor

$$\theta_x = 12\left(\frac{p_n}{\sigma_o}\right)\left(\frac{R}{c}\right)^2 \cdot \frac{\left(x_{cp} - x_t\right)}{t} \tag{23}$$

For the example vehicle

$$p_n = .0685 \times 10^{-6} \text{ lb/ft}^2$$

$$\sigma_o = 144,000 \text{ lb/ft}^2$$

$$R/c = 18,600/4.84 = 3840$$

$$t = .00025 \text{ in}$$

so that

$$\theta_x = 12 \times \frac{.0685 \times 10^{-6}}{.144 \times 10^{6}} \times (3840)^2 \times \frac{\left(x_{cp} - x_t\right)}{.00025}$$

$$= .336\left(x_{cp} - x_t\right) \text{ radians}$$

when $x_{cp} - x_t$ is expressed in inches.

The pitch angle at the tip is, using this result and figure 8,

$$\theta_{tip} = .1075\left(x_{cp} - x_t\right) \quad \text{radians}$$

It is clear that accurate control of the chordwise locations of the center of pressure and of the center of gravity is required to maintain blade trim. Equation (23) shows, furthermore, that the severity of the trim problem increases as blade aspect ratio is increased and as blade thickness is decreased.

A related problem is the tendency of the blade to camber, or curl, about a spanwise axis due to differential thermal expansion, differential Poisson's ratio expansion, and differential built-in strain. Calculation shows that the chordwise membrane stress, σ_x, is too small to prevent camber, but that chordwise battens spaced at approximately 100 foot intervals will probably result in a sufficiently smooth surface. The weight of the battens is estimated to be about 1% of the sail weight.

The differential equation that governs inplane (chordwise) deflection is

$$\frac{\partial^2}{\partial r^2}\left(EI\cdot\frac{\partial^2 u}{\partial r^2}\right) - \frac{\partial}{\partial r}\left(ct\sigma_r\cdot\frac{\partial u}{\partial r}\right) - \rho ct\Omega^2 u = cp_x \qquad (24)$$

where u is the inplane deflection and p_x is the inplane component of pressure. Note that the third term on the left represents a negative restoring spring. The net result of combining the second and third terms is to produce zero resistance to rigid-body rotation about the axis of spin and to produce positive resistance to inplane deformation.

The relative importance of bending stiffness may be determined by comparing the magnitudes of the first and second terms for an assumed deformation wavelength, λ_u. The result is

$$\frac{k_{bend}}{k_{c.f.}} = \frac{\pi^2}{3}\left(\frac{E}{\sigma_r}\right)\cdot\left(\frac{c}{\lambda_u}\right)^2 \qquad (25)$$

For the example vehicle

$E = 1.03 \times 10^6$ psi (composite modulus of Mylar-aluminum sandwich)

$\sigma_r = 750$ psi (at blade semi-span)

$c = 4.84$ ft

Thus

$$\frac{k_{bend}}{k_{c.f.}} = \frac{106,000}{(\lambda_u)^2} \tag{26}$$

where λ_u is in feet. The stiffness due to centrifugal force exceeds the stiffness due to bending for deformation wavelengths greater than 325 ft. Bending stiffness is important only during the initial stage of deployment.

Equation (24) has been used to compute the chordwise deformation of a blade that is subjected to 30 degrees of pitch at the root. It was assumed that blade twist conforms to the curve shown in figure 8 even at this relatively large angle. The inplane component of pressure is

$$p_x = p_o \cdot \sin\theta \cdot \cos^2\theta - \rho t r \dot{\Omega} \tag{27}$$

where the second term represents inertia relief. If it is assumed that all of the polar moment of inertia of the vehicle is in the blades, then it may be shown that

$$p_x = p_o \left\{ \sin\theta \cdot \cos^2\theta - \frac{3r}{R} \int_o^1 \sin\theta \cdot \cos^2\theta \cdot y dy \right\} \tag{28}$$

The net loading on the outboard portion of the blade is negative, causing the blade tip to lag behind a tangent to the blade axis at the root. Integration of equation (24) shows that, for an assumed 30 degree collective pitch displacement, the

lag distance for the blade tip is equal to

$$u_{tip} = .129\left(\frac{p_o}{\sigma_o}\right)\cdot\frac{R^2}{t} \tag{29}$$

For the example vehicle

$$p_o = .1882 \times 10^{-6} \text{ psf}$$

$$\sigma_o = .144 \times 10^{6} \text{ psf}$$

$$R = 18{,}600 \text{ ft}$$

$$t = 2.08 \times 10^{-5} \text{ ft}$$

so that

$$u_{tip} = .129 \times \frac{.1882 \times 10^{-6}}{.144 \times 10^{6}} \times \frac{(18600)^2}{2.08 \times 10^{-5}} = 2.81 \text{ ft} \tag{30}$$

The significance of this result can only be determined by a coupled analysis of vertical, inplane and twisting deformations. The main effect is to couple pitch and vertical deflection.

CONTROL CHARACTERISTICS

Conventional helicopter controls are used in an unconventional manner to produce all desired control responses of the heliogyro. The pitch angle of a rotor blade with conventional controls may be expressed as

$$\theta = \theta_o + a_1 \cdot \sin\left(\Omega t - \psi_o\right) + b_1 \cdot \cos\left(\Omega t - \psi_o\right) \qquad (31)$$

where θ_o, a_1 and b_1 are slowly varying functions of time and ψ_o is an azimuth reference that is fixed in the non-rotating system. Usually ψ_o is chosen to coincide with the longitudinal axis of the vehicle. θ_o is called the collective pitch angle. a_1 and b_1 are called the longitudinal and lateral components of cyclic pitch.

The use of cyclic pitch to produce a steady component of force in the plane of the rotor is illustrated in figure 9a. The use of combined collective and cyclic pitch to produce a steady rolling moment on the rotor is illustrated in figure 9b. In the figure, the vertical components of the forces on the blades in positions 1 and 3 are equal, whereas the vertical component of force on the blade in position 4 obviously exceeds that on the blade in position 2 .

Collective pitch also produces spin torque and reduction of the component of force normal on the rotor plane as may be seen from figure 10.

A quantitative analysis of the forces and moments acting on the rotor should include a consideration of the steady coning angle, β , and of the angle, γ , between the direction of illumination and the axis of rotation. These angles and the coordinate geometry of a rotating blade are shown in figure 11.

The derivation of equations for the forces and moments acting

on the rotor, which is straightforward even if somewhat tedious, is outlined in the Appendix. Results that are important for a preliminary evaluation of the heliogyro are summarized in Table 2.

The control characteristics of the heliogyro will be illustrated by a series of sample calculations applied to the example vehicle of the preceding section. Consider first the rate at which rotational speed of a two-bladed rotor can be changed by collective pitch for the condition of no coning and normal incidence of the solar illumination. From Table 2, (case 7);

$$M_z = 2p_o cR^2 \int_o^1 \sin\theta_o \cdot \cos^2\theta_o y \cdot dy \qquad (32)$$

The integral appearing in this equation is evaluated by means of the universal blade twist curve shown in figure 8. If, for example, the collective pitch angle imposed at the blade root is 30 degrees, the value of the integral is equal to 0.1202 . For the example vehicle in Earth orbit

$$p_o = 1.882 \times 10^{-6} \text{ lb/ft}^2$$

$$cR = 90{,}000 \text{ ft}^2$$

$$R = 18{,}600 \text{ ft}$$

so that, for $\theta_{root} = 30°$,

$$M_z = 2 \times .1882 \times 10^{-6} \times (90{,}000) \times 18{,}600 \times .1202$$

$$= 75.9 \text{ ft-lbs}$$

The time required to go from zero to full speed is

$$t = \frac{\Omega I}{M_z} \qquad (33)$$

where I is the polar moment of inertia of the vehicle.

The rotational speed may be obtained from the rotational

period, τ , plotted in figure 7. For the example vehicle with 1000 psi blade root stress, τ is approximately equal to six minutes which gives $\Omega = .0175$ rad/sec. The polar moment of inertia of the example vehicle is equal to 1.28×10^9 lb-sec^{2}ft. Thus the spin-up time is

$$t = \frac{.0175 \times 1.28 \times 10^9}{75.9} = 288{,}000 \text{ seconds} = 3.34 \text{ days.}$$

Consider next the rate at which the spin axis can be precessed by the simultaneous application of collective and cyclic pitch. From Table 2, (case 5), for zero coning and normal incidence of the solar illumination,

$$M_y = 3p_o b_1 cR^2 \int_o^1 \sin\theta_o \cdot \cos^2\theta_o y \cdot dy \qquad (34)$$

If the collective pitch angle at the root is again taken to be 30 degrees, the precessional moment is

$$M_y = \frac{3}{2} \cdot b_1 \times 77.9 = 114 b_1 \text{ ft-lbs}$$

The precessional rate is

$$\dot{\theta}_x = \frac{M_y}{\Omega I} = \frac{114 b_1}{.0175 \times 1.28 \times 10^9} = 5.2 \times 10^{-6} \times b_1 \text{ rad/sec}$$

$$= 25.7 b_1 \text{ degrees/day}$$

If the cyclic pitch angle, b_1 , is taken to be 10 degrees then $\dot{\theta}_x = 4.48$ degrees per day, which is more than sufficient for the requirements of interplanetary travel.

Since collective pitch produces spin torque, the precessional maneuver will be accompanied by an undesirable change in the spin rate. Large changes in spin rate can, however, be avoided by periodically reversing the signs of both the cyclic and collective pitch angles during the precessional maneuver. It is seen,

from equation (34) that the direction of the precessional torque remains unchanged if both cyclic and collective pitch are reversed.

It is shown in Table 2 (case 2) that coning produces a steady moment tending to precess the spin axis in a cone about the direction of the illumination. The magnitude of the moment for the example vehicle is, assuming the coning angle to be uniform along the blade span

$$M_y = \frac{1}{2} \cdot p_o c R^2 \cdot \sin 2\gamma \cdot \sin\beta \qquad (35)$$

The coning angle for the example vehicle was previously shown to be equal to .000425 radians for a blade root stress equal to 1000 psi. If the illumination angle, γ, is set equal to its best value (35° 15.9'), the resulting moment is .063 ft-lbs and the resulting precessional rate is .0143 degrees per day, which is barely large enough to require occasional correction on a long voyage. If the spin rate were decreased by a factor of ten, however, the precessional rate would be increased by a factor of 1000.

DEPLOYMENT

A suggested deployment sequence for two-bladed vehicles is shown in figure 10. The vehicle is oriented in a plane perpendicular to the illumination and a rocket motor is ignited. The resulting spin provides centrifugal force to keep the blades taut while they are initially unrolled. It is impractical to provide more than a small fraction of the total angular momentum by initial spin. After the blades have been unrolled to a small distance, they are pitched collectively and then gradually unrolled as photon pressure increases the angular momentum.

Design criteria for the initial deployment radius and for the subsequent rate of change of radius are provided by the requirements for blade straightness and for blade trim.

Equation (18) shows that the ratio of blade radius to blade root stress should be kept constant in order to keep the coning angle constant. The requirement for blade twisting deformation, equation (23), is less severe at reduced blade radii and the

requirement for blade inplane deformation is of equal severity. Thus, if the same criteria are applied to blade deformations during and after deployment, the ratio R/σ_o should be kept constant. Since σ_o is proportional to $(R\Omega)^2$, it is implied that the centripetal acceleration $R\Omega^2$ should be kept constant during deployment.

The resulting formulas for initial deployment radius and for the time required to complete the gradual payout phase are

$$R_1 = R_f\left(\frac{I_o\Omega_o}{I_f\Omega_f}\right)^{2/5} \tag{36}$$

and

$$t_2 = 5\cdot\frac{I_f\Omega_f}{M_{zf}}\left[1 - \sqrt{\frac{R_1}{R_f}}\right] \tag{37}$$

where subscript (o) refers to conditions existing after initial spin-up but prior to initial payout and subscript (f) refers to final conditions.

Let it be assumed that the two-bladed example vehicle is initially spun up until the radial acceleration is equal to six g's at a distance that is 3 feet from the center of rotation. Estimating the polar moment of inertia of the undeployed configuration to be 80 lb-sec^2-ft and using results of preceding calculations, it is found that

Initial angular velocity: $\Omega_o = 11.36$ rad/sec

Initial angular momentum: $I_o\Omega_o = 908$ lb-ft-sec

Total impulse at 3.5 ft radius: 260 lb-sec

Final angular momentum: $I_f\Omega_f = 2.24 \times 10^7$ lb-ft-sec

Rotor torque at full radius for 30 degrees of collective pitch: $M_{zf} = 75.9$ ft-lbs

Initial payout radius: $R_1 = 326$ ft

Time for gradual payout: 14.5 days.

During initial deployment the angular momentum of the payload package is transferred to the unrolling blades. Since the radius is small, moment is transferred to the blades primarily by chordwise bending. If it is required that there be no compression in the trailing edges of the blades, then it can be shown that the initial payout rate is limited to

$$\frac{dR}{dt} < \frac{\Omega_o c}{12} \tag{38}$$

Thus it is required for the present example that

$$t_1 > \frac{12R_1}{\Omega_o c} = \frac{12 \times 326}{11.36 \times 4.84} = 71.2 \text{ seconds}$$

MANEUVERS IN PLANETARY ORBIT

An important and difficult maneuver that has received considerable attention in the literature on solar sails, is the planetary escape maneuver, references 2, 5, and 6. The reasons for the difficulty are that the gravitational attraction in a low planetary orbit is much larger than the solar radiation pressure and that special means are required to derive an increment of angular momentum from the sun during each revolution around the planet.

Two proposed planetary escape maneuvers for the heliogyro are shown in figure 12. In figure 12a the vehicle is placed into a circular polar orbit with both the plane of the orbit and the plane of the vehicle normal to the direction of illumination. Cyclic pitch is used to generate a force in the direction of orbital motion by the means illustrated in figure 9a.

A formula for the magnitude of the inplane force due to cyclic pitch is given in Table II, case 9, for the condition of uniform blade pitch along the span. It is reasonable to assume uniform blade pitch along the span because the frequency of pitch oscillation is nearly equal to one cycle per revolution in the rotating system and, as a result, the distributed centrifugal restoring moment is nearly cancelled by the distributed inertia moment. (See discussion following equation (21)). Evaluation of the formula given in Table II shows that the maximum inplane force is achieved for a cyclic pitch angle near $45°$ but that the inplane force for a pitch angle equal to $30°$ is only slightly less. Assuming then, that the cyclic pitch amplitude is equal to $30°$, the resulting inplane force on a two-bladed rotor is equal to

$$F_{\psi} = .205 p_o A \tag{39}$$

where p_o is the solar radiation pressure and A is the total surface area.

In figure 12b the vehicle is placed in an equatorial orbit with the plane of the rotor normal to the direction of illumination.

Both cyclic and collective pitch are employed during each orbital revolution to produce a net average force in the direction of orbital motion. Let it be assumed that the root collective pitch angle in quadrant (4) is $60°$ and that the cyclic pitch angle in quadrants (1) and (3) is $30°$. The axial force in quadrant (4) obtained with the aid of the universal collective pitch curve, figure 8, is

$$F_z = .521 p_o A \tag{40}$$

The average force in the direction of orbital motion is

$$F_\psi = \frac{p_o A}{2\pi}\left[4\int_0^{45°} .205\cdot\cos\varphi\cdot d\varphi + 2\int_{45°}^{90°} (1 - .521)\cdot\sin\varphi\cdot d\varphi\right] \tag{41}$$

$$= .200 p_o A$$

Comparison of equations (39) and (41) shows that the forces available for planetary escape in the polar and equatorial orbits are about equal. Slightly larger thrusts are possible with more complicated maneuvers. For example, the regions of collective and cyclic pitch could be overlapped in the equatorial orbit, or the axis of rotation could be precessed to provide a favorable orientation of the entire vehicle. The analysis of precession rates presented in the preceding section shows, however, that the obtainable precession angle is too small to be significant except for very high orbits.

An approximate analysis of circular planetary orbits shows that the time to escape the planet from an initial orbital altitude, h_i, above the surface is

$$t_e = \frac{m_v g_o^{1/2} r_o}{F_\psi \left(h_i + r_o\right)^{1/2}} \tag{42}$$

where F_ψ is the average force in the direction of orbital motion, m_v is the mass of the vehicle, and g_o is the

gravitational acceleration at the surface of the planet whose radius is r_o .

Equation (42) is reasonably accurate provided that the gravitational attraction of the planet at the initial orbital altitude is large compared to F_ψ .

Substituting for F_ψ from equation (41):

$$t_e = \frac{5m_v}{p_o A} \cdot \frac{g_o^{1/2} r_o^{1/2}}{\left(1 + \frac{h_i}{r_o}\right)^{1/2}} \tag{43}$$

or, using equation (7) for operation within the Earth's gravitational field,

$$t_e = \frac{5}{.611 \times 10^{-3} \lambda} \cdot \frac{r_o^{1/2}}{g_o^{1/2}\left(1 + \frac{h_i}{r_o}\right)^{1/2}}$$

$$= \frac{76.3}{\lambda\left(1 + \frac{h_i}{r_o}\right)^{1/2}} \quad \text{days} \tag{44}$$

This result is plotted in figure 13. The importance of lightness number with regard to the time for planetary escape is clear. For manned interplanetary voyages, it is probably desirable to have the vehicle climb in an unmanned condition from a low Earth orbit to a fairly high one in order to minimize radiation hazard in the Van Allen belt.

Figure 13 also shows that the changes in the Earth's position with respect to the sun during the escape maneuver is sufficiently large to invalidate the assumption of normal illumination used in the analysis of planetary escape from polar orbit. As a result, escape from an initially polar orbit is actually more complicated than escape from an equatorial orbit and will probably turn out to be less useful.

The escape time for planets other than Earth may be calculated using equation (43). The escape times for the first six planets, relative to the escape time from Earth, are tabulated in Table III. It is clear from examination of the table, that entry of a solar sail into a low orbit around the planets beyond Mars is impractical. The escape time from Mars is, interestingly enough, about equal to the escape time from Earth.

Another useful maneuver is the ability to change position in a given orbit. Such a maneuver might, for example, be used to provide periodic visits to a number of satelites in a synchronous orbit. The simplest method for providing a change in orbital azimuth is to exert a force, F_ψ, in the direction of motion for an interval of time, Δt, and then to reverse the direction of force for a like interval of time. The time required to provide an azimuth change of magnitude $\Delta\psi$ is

$$t_m = 2\Delta t = \frac{2}{\sqrt{3}}\left(\frac{m_v r_i}{F_\psi}\cdot\Delta\psi\right)^{1/2} \tag{45}$$

Substituting for F_ψ from equation (41)

$$t_m = \frac{2}{\sqrt{3}}\left(\frac{5m_v}{p_o A}\cdot r_i\Delta\psi\right)^{1/2} \tag{46}$$

or, using equation (7) for operation within the Earth's gravitational field,

$$t_m = \frac{2}{\sqrt{3}}\left(\frac{5r_i\Delta\psi}{.611\times 10^{-3} g_o\lambda}\right)^{1/2}$$

and, after some manipulation,

$$t_m = .976\left(\frac{r_i}{r_o}\cdot\frac{\Delta\psi}{\lambda}\right)^{1/2} \quad \text{days} \tag{47}$$

As an example, consider a synchronous orbit, such that $r_i/r_o = 6.6$, and the example vehicle of the preceding sections which has a lightness number equal to 0.1. Let the desired change in orbital position be 180°. Then

$$t_m = .976 \left(6.6 \times \frac{\pi}{0.1} \right)^{1/2} = 14.1 \quad \text{days} \qquad (48)$$

ADVANCED CONFIGURATIONS

Preliminary designs for advanced configurations of large size have been explored in order to illustrate the performance and load carrying capabilities of the heliogyro concept for long voyages in space. The principal constraints in selecting vehicle size have been the dimensional and payload weight capabilities of the Saturn V booster system. Accordingly, the gross weight of the spacecraft has been chosen to be 100,000 lbs and the dimensions of the stowed configuration have been selected to fit within a cylinder that is sixty feet long and twenty feet in diameter.

It has been assumed that .05 mil Mylar (or an equivalent light-weight material) will be available in the desired quantity for the construction of the blades. For such material, figures 1, 2 and 13 show that a good compromise between performance and load carrying capability is obtained with a lightness number equal to 0.3 and a payload weight fraction equal to .484 . Once gross weight and lightness number have been specified, the required sail area is computed by means of equation (6). The result is

$$A = \frac{W\lambda}{.308 \times 10^{-3}} = \frac{100{,}000 \times 0.3}{.308 \times 10^{-3}} = 97.5 \times 10^6 \quad \text{ft}^2 \qquad (49)$$

The arrangement of the components in a large heliogyro system is largely a matter of the application of design ingenuity to the packaging and deployment requirements. It has been assumed that automatic deployment from a single container is mandatory.

The general arrangement of the first of two proposed configurations is shown in figure 14. The system consists of an axisymmetric array of blades connected to a structural ring, and a centrally located payload capsule that is attached to the ring by means of cables. The ring is divided into twenty-four segments, separated by hinges. The hinges are mechanically actuated and

kept in synchronism during deployment by a control cable within the ring. The cables supporting the central capsule are payed out under tension during deployment. An electrical motor that supplies blade pitch is located at the center of each ring segment. A detailed sketch of the stowed configuration is shown in figure 15.

The tip radius of the blades satisfies the relationship

$$R = \frac{A}{n_b c} > \frac{A}{\pi D_r} \tag{50}$$

where D_r is the diameter of the hinged ring. It is, therefore, desirable to make the ring diameter large in order to minimize the tip radius. The ring diameter is, on the other hand, limited by the volume available for the stowed configuration. The chosen value (336 feet) provides a circumference equal to 1057 feet of which 90% is used for the attachment of 96 ten-foot-chord blades. The resulting blade tip radius is 101,400 feet.

Operational characteristics of the pin-wheel model (rotational period, tip speed and coning angle) are given in Table IV for a blade root stress equal to 3000 psi. Final deployment from the unfolded ring condition is achieved in a manner similar to that for the experimental two-bladed model. The configuration is first spun up by rocket motors to produce a moderate radial acceleration; the blades are then unrolled to a predetermined radius, pitched, and gradually payed out as photon pressure increases angular momentum. The estimated time for deployment, as computed by equation (37), is about eight days.

The general arrangement of the second configuration is shown in figure 16. The system consists of a number of parallel blades with two payload capsules located half-way from the center to the blade tips. The pitch mechanisms of the blades are slaved together by a control cable that is driven by an electric motor. The blades between the two capsules are not moveable. All of the blades are attached to booms that extend from the payload capsules and that are hinged to permit folding into the stowed configuration.

The axes of the moveable blades are directed toward the center of rotation. The axes of the fixed blades are curved slightly outward from the center of rotation due to the action of centrifugal force.

A detailed view of the stowed configuration is shown in figure 17. The main effect of restricted packaging volume is to limit the length of the blade attachment booms, which have been selected to have an overall length equal to 500 feet. Each boom segment carries four ten-foot-wide blades per side which could, if desired, be replaced by a single forty-foot wide blade. The total tip-to-tip span of the blades is 244,000 feet, or about 46 miles.

One important design feature of the parallel blade configuration is that artificial gravity is provided within the payload capsules. Design data given in Table IV show that, if the blade root stress is equal to 5000 psi, the artificial gravity is equal to .066 g's. The most effective means for providing a larger centrifugal force field is to increase blade stress, which would require the development of a suitable material that is stronger than Mylar.

It will be noted that the centrifugal load on the payload capsules is supported by cables rather than being beamed to the blades. The main reason for this arrangement is that the increased load in the blades would require a reduction by about a factor of two in the artificial gravitational field. The estimated weight of the cables, if made from unidirectional glass laminate and stressed to 100,000 psi, is about 2000 pounds.

An artist's view of one of the payload capsules is shown in figure 18. Also visible in the figure are a cable-car for transportation to the other payload capsule and a smaller docked spacecraft.

Other features of the parallel blade configuration that are considered to be important for long manned space voyages are the accessibility of all moving parts, and the roominess of the crew compartments.

The deployment sequence is as follows: After the blade support booms have been unfolded, the configuration is spun up by means of rocket motors at the boom tips. The non-moveable blades are then payed out to a predetermined distance, after which the moveable blades are payed out a small distance and pitched. Finally both sets of blades are gradually payed out as photon pressure increases angular momentum. Lag hinges for the moveable blades must be provided in order to permit their axes to point

toward the center of rotation during deployment.

MISSIONS

The missions for which solar sails are best suited are quite obviously those for which the total impulse is large and the maximum required thrust is low, which means, among other things, missions of long duration. Electric propulsion schemes are similar to the solar sail in these respects, and are competitive with it for missions of moderate duration.

It is of interest to determine the characteristics of an ion engine with the same thrust capability as the advanced heliogyro configurations described in the preceding section. The fundamental equation of an inertial reaction motor is that the thrust

$$T = (2P\dot{m})^{\frac{1}{2}} \tag{51}$$

where P is the power dissipated and $\dot{m}$ is the mass flow rate. It is clear that in designing an ion engine a compromise between power dissipation and fuel weight must be made. Another useful relationship is that the power

$$P = \frac{1}{2} \cdot T \cdot V = \frac{1}{2} \cdot T \cdot I_{sp} g \tag{52}$$

where V is the velocity of expelled particles and I_{sp} is the specific impulse.

The total photon force acting on the advanced heliogyro configurations of the preceding section in the vicinity of the Earth is

$$F = p_o A = .1882 \times 10^{-6} \times 97.5 \times 10^{6} = 18.4 \text{ lbs} \tag{53}$$

Assuming that, on average, one-third of the total force is

available as useful thrust, the thrust of the comparable ion engine is 6.13 lbs. Assuming that the ion engine has a specific impulse equal to 6000 sec, the required power is, from equation (52), $.592 \times 10^6$ ft-lbs/sec or 805 KW. The weight assignable to the generation of power, assuming a SNAP 50 type power plant with 80% propulsive efficiency is about 35,000 lbs. The mass flow rate is, from equation (51)

$$\dot{m} = \frac{T^2}{2P} = \frac{(6.13)^2}{2 \times .592 \times 10^6} = 31.7 \times 10^{-6} \text{ slugs/sec} \qquad (54)$$

If 30,000 lbs of fuel are expended at this rate, the fuel will be exhausted in 29.4×10^6 sec or in about one year. Thus, considering the fact that 65,000 lbs of fuel and propulsion weight are required with the ion engine compared with a total weight of about 60,000 lbs assignable to propulsion with the advanced heliogyro, the heliogyro shows definite advantage over ion propulsion for missions requiring more than one year of sustained thrust. Included in such missions are a round trip to Mars.

Other missions besides interplanetary voyages for which the heliogyro might be advantageous are station-keeping, station visiting, and space-junk collection in Earth orbit. The size of the solar sail required for station keeping is very much smaller than those that have been considered in previous sections. It is stated in reference 13, for example, that a 1500 lb satellite in synchronous orbit would require about 200 dynes of maximum thrust. Calculations show that this thrust level can be achieved with about 10,000 square feet of sail area. The sail weight, assuming ¼ mil aluminized Mylar would be about 20 lbs, which is substantially smaller than the values quoted in reference 13 for competing chemical and electrical propulsion schemes. The infinite (or at least very long) life of the solar propulsion scheme is an additional advantage.

The use of the heliogyro for station visiting missions has been discussed in the section on Maneuvers in Planetary Orbit. A competing chemical propulsion system with a comparable payload to weight ratio would be exhausted of fuel after a relatively small number (about 25) of starts and stops.

As a final exercise, consider a voyage to Mars in which the space-craft descends into a low Martian orbit, climbs back out

and returns to Earth as fast as possible. The mission involves the following phases

a) Injection into a low Earth orbit
b) Climb, in an unmanned condition, to a 20,000 mile orbit
c) Voyage to Mars on a capture trajectory
d) Descent to a low Martian orbit and return
e) Voyage back to Earth on a fly-by trajectory.

The elapsed time for the mission can be computed as a function of lightness number by means of figures 1 and 13, and Table III. The resulting total time for the manned portion of the mission is shown in figure 19.

CONCLUDING DISCUSSION

Design concepts for a new type of space vehicle have been introduced and some of the engineering problems associated with its deployment and operation have been considered in this report. It is hoped that the reader has been impressed with the performance potential of the heliogyro and that he is not overly skeptical with regard to its technical feasibility.

Much work remains to be done before technical feasibility can be established with reasonable assurance. One of the areas of greatest concern is the effect of blade deformations on controllability. It has been shown, for example, that in the absence of bending deformations, a collective pitch angle imposed at the root of a blade is propagated to the tip of the blade by centrifugal stiffening. The extent to which flapwise and chordwise deformations interfere with the spanwise propagation of blade pitch is not known at present. A fully coupled analysis, including dynamic effects, is required in order to obtain such knowledge. One of the results of the coupled analysis could be the existance of a practical limit on blade aspect ratio beyond which the ability to control blade pitch rapidly deteriorates. The aspect ratios for the sample designs considered in the report are in the range from 3800 to 10,000. They could, if necessary, be lowered to approximately 1000 without major effect on stowed volume, simply by increasing blade chord.

Although currently available materials appear to be adequate for the design of heliogyro blades, significant increases in

performance could be obtained with better materials. Reduction of film thickness is an obvious goal that will produce either shorter mission times or larger payload weight fractions. The development of films with higher strength is also desirable, particularly for larger vehicles. The higher spin rates permitted by higher strength materials will result in a larger artificial gravity for manned vehicles and in an improvement of controllability.

It would appear that the weight and performance advantages of the heliogyro for long space missions are sufficient reasons for the expenditure of additional effort on its development. An additional inducement is the relative simplicity of the hardware, when compared to various forms of electric propulsion. It is perhaps not too much to claim that, if anyone journeys to Mars in this century, he will go by solar sail and, more particularly, by a version of the heliogyro.

Astro Research Corporation,
Santa Barbara, California, March 13, 1967.

APPENDIX

DERIVATION OF EQUATIONS FOR THE FORCES AND MOMENTS ON A ROTOR DUE TO SOLAR ILLUMINATION

Figure 11 shows the coordinate geometry for a rotating blade that is coned through an angle β with respect to the plane of rotation and subsequently pitched through an angle θ with respect to a tangent to the cone of rotation. The illumination lies in the x-z plane at an angle γ with respect to the axis of rotation.

The radiation pressure is assumed to act normal to the surface of the blade with magnitude

$$p_n = p_o \cos^2\alpha \tag{A-1}$$

where α is the angle between the normal to the surface and the direction of illumination.

Let the direction cosines of the normal in the non-rotating coordinate system be a_x, a_y, and a_z, and the direction cosines of the direction of illumination be b_x, b_y, and b_z. Then

$$p_n = p_o\left|a_x b_x + a_y b_y + a_z b_z\right|^2 \tag{A-2}$$

The direction cosines of the illumination are:

$$\begin{aligned} b_x &= \sin\gamma \\ b_y &= 0 \\ b_z &= \cos\gamma \end{aligned} \tag{A-3}$$

The direction cosines of the normal in the blade $(\bar{x}\ ,\ \bar{y}\ ,\ \bar{z})$ coordinate system are:

$$\left.\begin{aligned} \bar{a}_x &= \sin\theta \\ \bar{a}_y &= -\cos\theta\cdot\sin\beta \\ a_z &= \cos\theta\cdot\cos\beta \end{aligned}\right\} \qquad \text{(A-4)}$$

so that, in the non-rotating coordinate system

$$\left.\begin{aligned} a_x &= \bar{a}_x\cdot\sin\psi + \bar{a}_y\cdot\cos\psi \\ &= \sin\theta\cdot\sin\psi - \cos\theta\cdot\sin\beta\cdot\cos\psi \\ a_y &= -\bar{a}_x\cdot\cos\psi + \bar{a}_y\cdot\sin\psi \\ &= -\sin\theta\cdot\cos\psi - \cos\theta\cdot\sin\beta\cdot\sin\psi \\ a_z &= \cos\theta\cdot\cos\beta \end{aligned}\right\} \qquad \text{(A-5)}$$

The pressure on the blade is, substituting into equation (A-2),

$$p_n = p_o\left[(\sin\theta\cdot\sin\psi - \cos\theta\cdot\sin\beta\cdot\cos\psi)\ \sin\gamma + \cos\theta\cdot\cos\beta\cdot\cos\gamma\right]^2 \qquad \text{(A-6)}$$

The components of pressure in the $(x\ ,\ y\ ,\ z)$ system are:

$$\left.\begin{aligned} p_x &= a_x p_n \\ p_y &= a_y p_n \\ p_z &= a_z p_n \end{aligned}\right\} \qquad \text{(A-7)}$$

The components of pressure in, and perpendicular to, the direction of illumination (lift and drag components) are:

$$\begin{aligned} p_\ell &= -p_x\cos\gamma + p_z\cdot\sin\gamma = (-a_x\cdot\cos\gamma + a_z\cdot\sin\gamma)\cdot p_n \\ p_d &= p_x\cdot\sin\gamma + p_z\cdot\cos\gamma = (a_x\cdot\sin\gamma + a_z\cdot\cos\gamma)p_n \end{aligned} \qquad \text{(A-8)}$$

The pressure-moments about the x , y , and z axes are:

$$m_x = - p_y r \cdot \tan\beta + p_z r \cdot \sin\psi$$
$$= r\left(\sin\theta \cdot \cos\psi \cdot \tan\beta + \frac{\cos\theta}{\cos\beta} \cdot \sin\psi\right) p_n \qquad \text{(A-9)}$$

$$m_y = p_x r \cdot \tan\beta - p_z r \cdot \cos\psi$$
$$= r\left(\sin\theta \cdot \sin\psi \cdot \tan\beta - \frac{\cos\theta}{\cos\beta} \cdot \cos\psi\right) p_n \qquad \text{(A-10)}$$

$$m_z = p_x r \cdot \sin\psi + p_y r \cdot \cos\psi$$
$$= - r \cdot \sin\theta \cdot p_n \qquad \text{(A-11)}$$

The average forces and moments acting on the rotor are, assuming constant chord blades

$$F_j = \frac{n_b c}{2\pi} \int_o^{2\pi} \int_o^R p_j \, d\psi \, dr \qquad j = x, y, z \qquad \text{(A-12)}$$

and

$$M_j = \frac{n_b c}{2\pi} \int_o^{2\pi} \int_o^R m_j \, d\psi \, dr \qquad j = x, y, z \qquad \text{(A-13)}$$

where n_b is the total number of blades and c is the blade chord.

Due to the complexity of the resulting expressions,

immediate interest centers in special cases wherein one or more of the angles β, γ, and θ are assumed to be small or zero. Useful results for special cases are summarized in Table II.

REFERENCES

1. Wiley, C. (pseudonym: Saunders, R.) "Clipper Ships of Space", Astounding Science Fiction, May 1951, p. 135.
2. Cotter, T. "Solar Sailing" Sandia Corporation Research Coloquium SCR-78, April 1959, Office of Technical Services, Dept. of Commerce, Washington D. C.
3. Garwin "Solar Sailing, A Practical Method of Propulsion within the Solar System", Jet Propulsion, March 1958.
4. Tsu, T. "Interplanetary Travel by Solar Sails" ARS Journal, June, 1959.
5. Villers, P. "On the Application of Solar Radiation Momentum Transfer to Space Vehicle Propulsion", M.S. Thesis, Mass. Inst. of Tech., Jan. 1960.
6. Gordon, B. J. "A Study of Interplanetary Travel by Solar Sail", M. S. Thesis, Air University, USAF, Wright-Patterson Air Force Base, Ohio, Aug., 1961.
7. Kelley, H.J. "Gradient Theory of Optimal Flight Paths" ARS Journal, Vol. 30, p. 947-954, Oct. 1960.
8. Wehner, G. K., Kenknight, C., and Rosenberg, D. L., "Sputtering Rates Under Solar-Wind Bombardment", Planetary Space Sci., Vol 11, pp. 885-895, 1963.
9. Wood, G., and Carter, A. F., "The Design Characteristics of Inflatable Aluminized-Plastic Spherical Earth Satellites with Respect to Ultraviolet, Visible, Infrared and Radar Radiation", ASME Paper 59-AV-38.
10. Jahsman, W. E. "Mass Considerations in Ring-Supported Solar Sails" General Research in Flight Sciences, Vol III, Lockheed Missiles and Space Division Report No. LMSD-288139, Jan. 1960.
11. Robbins, W. J. Jr. "Electromagnetic Forces on Space Structures", NASA Contractor Report CR-476, May, 1966.
12. Schuerch, H. U., and MacNeal, R. H. "Deployable Centrifugally Stabilized Structures for Atmospheric Entry from Space", NASA Contractors Report CR-69, July, 1964.
13. Cheng, S. I. "Sputtering as an Advanced Concept of Space Propulsion" Astronautica Acta, Vol. 12, No. 4, July-August 1966, p. 272.

TABLE I

TECHNICAL CHARACTERISTICS OF EXPERIMENTAL TWO-BLADED HELIOGYRO

Gross Weight	550 lbs
Non-Sail Weight	200 lbs
Lightness Number	0.1
Blade Material	¼ mil Mylar with 1500 A° aluminum coating, each side
Blade Area	180,000 ft^2
Blade Tip Radius	18,600 ft
Blade Chord	4.84 ft
Rotational Period	6 minutes
Blade Root Stress	1000 psi
Blade Tip Speed	326 ft/sec
Root Coning Angle	.000425 radians
Polar Moment of Inertia	1.28×10^9 $lb\text{-}sec^2\text{-}ft$

TABLE II

SUMMARY OF CONTROL CHARACTERISTICS

Refer to Figure 11 for definitions of the angles β, γ, θ and ψ.

Case 1: Steady Flight with no coning ($\beta = \theta = 0$).

Lift: $L = p_o n_b \cdot Rc \cdot \sin\gamma \cdot \cos^2\gamma$

Drag: $D = p_o n_b Rc \cdot \cos^3\gamma$

Case 2: Longitudinal Moment due to coning in steady flight

$$M_y = \frac{1}{2} \cdot p_o n_b c \cdot \sin 2\gamma \int_o^R r \cdot \sin\beta \cdot dr$$

Case 3: Cyclic Pitch Required to achieve zero longitudinal moment in steady flight. β = constant; $\theta = a_1 \sin\psi$ where a_1 is small.

$$a_1 = \frac{-\sin 2\gamma \cdot \cos\beta}{\cos^2\beta \cdot \cos^2\gamma + \frac{1}{4} \cdot \sin^2\gamma}$$

Case 4: Combined cyclic and collective pitch required to achieve zero longitudinal moment in steady flight, β = constant; $\theta = \theta_o + b_1 \cdot \cos\psi$ where θ_o and b_1 are small and constant along the span.

$$\theta_o \cdot b_1 = \frac{-\sin\beta \cdot \sin 2\gamma}{3 \cdot \cos^2\gamma - \frac{1}{2} \cdot \sin^2\gamma}$$

Case 5: Longitudinal Control Moment for no coning; $\beta = 0$, $\theta = \theta_o + b_1 \cos\psi$ where b_1 is small and constant along the span

$$M_y = \frac{3}{2} \cdot p_o b_1 n_b c \int_o^R \sin\theta_o \cdot \cos^2\theta_o \left\{ \cos^2\gamma - \frac{1}{6} \cdot \sin^2\gamma + \frac{1}{12} \cdot \tan^2\theta_o \cdot \sin^2\gamma \right\} r dr$$

Case 6: Lateral Control Moment for no coning; $\beta = 0$, $\theta = \theta_o + a_1 \sin\psi$ where a_1 is small

$$M_x = \frac{3}{2} \cdot p_o n_b c \int_o^R \sin\theta_o \cdot \cos^2\theta_o \left\{ \sin 2\gamma - a_1 \left(\cos^2\gamma - \frac{1}{2} \cdot \sin^2\gamma + \frac{1}{4} \cdot \tan^2\theta_o \cdot \sin^2\gamma \right) \right\} r dr$$

Case 7: Spin Control Moment for no coning; $\beta = 0$, $\theta = \theta_o$

$$M_z = - p_o n_b c \int_o^R \sin\theta_o \cdot \cos^2\theta_o \left(\cos^2\gamma + \frac{1}{2} \cdot \tan^2\theta_o \cdot \sin^2\gamma \right) r dr$$

Case 8: Control Forces for no coning and normal incidence of illumination; $\beta = 0$, $\gamma = 0$, and $\theta = \theta_o + b_1 \cos\psi$ where b_1 is small and constant along the span

$$F_y = - \frac{1}{2} \cdot p_o b_1 n_b c \int_o^R \left(\cos^3\theta_o - \sin^2\theta_o \cdot \cos\theta_o \right) dr$$

$$F_z = p_o n_b c \int_o^R \cos^3\theta_o dr$$

Case 9: Lateral Control Force for no coning and normal incidence of illumination; $\beta = 0$, $\gamma = 0$ and $\theta = b_1 \cos\psi$ where b_1 is not small but is constant along the span

$$F_y = -\frac{1}{2} \cdot p_o n_b Rc \left[b_1 - .875 b_1^3 + .318 b_1^5 + - - \right]$$

TABLE III

RELATIVE TIMES TO ESCAPE FROM
PLANETARY ORBIT BY SOLAR SAIL

Planet	$\frac{\text{Time to Escape from Planet}}{\text{Time to Escape from Earth}}$
Mercury	.056
Venus	.479
Earth	1.000
Mars	1.06
Jupiter	128.
Saturn	295.

TABLE IV

TECHNICAL CHARACTERISTICS OF ADVANCED CONFIGURATIONS

Item	Unmanned Pinwheel Model	Manned Parallel Blade Model
Gross Weight (lbs)	100,000	100,000
Non-sail Weight (lbs)	48,400	48,400
Lightness Number	0.3	0.3
Blade Material	1/20 mil Mylar with 1500°A aluminum coating, each side	
Blade Area (ft^2)	97.5×10^6	97.5×10^6
Number of Moveable Blades	96	80
Number of Fixed Blades	0	40
Blade Tip Radius (ft)	101,400	122,000
Blade Chord (ft)	10	10
Rotational Period (min)	18.4	17.5
Artificial Gravity for Passenger's (g's)	0	.066
Blade Root Stress (psi)	3000	5000
Blade Tip Speed (ft/sec)	568	732
Root Coning Angle (radians)	.0048	.00237

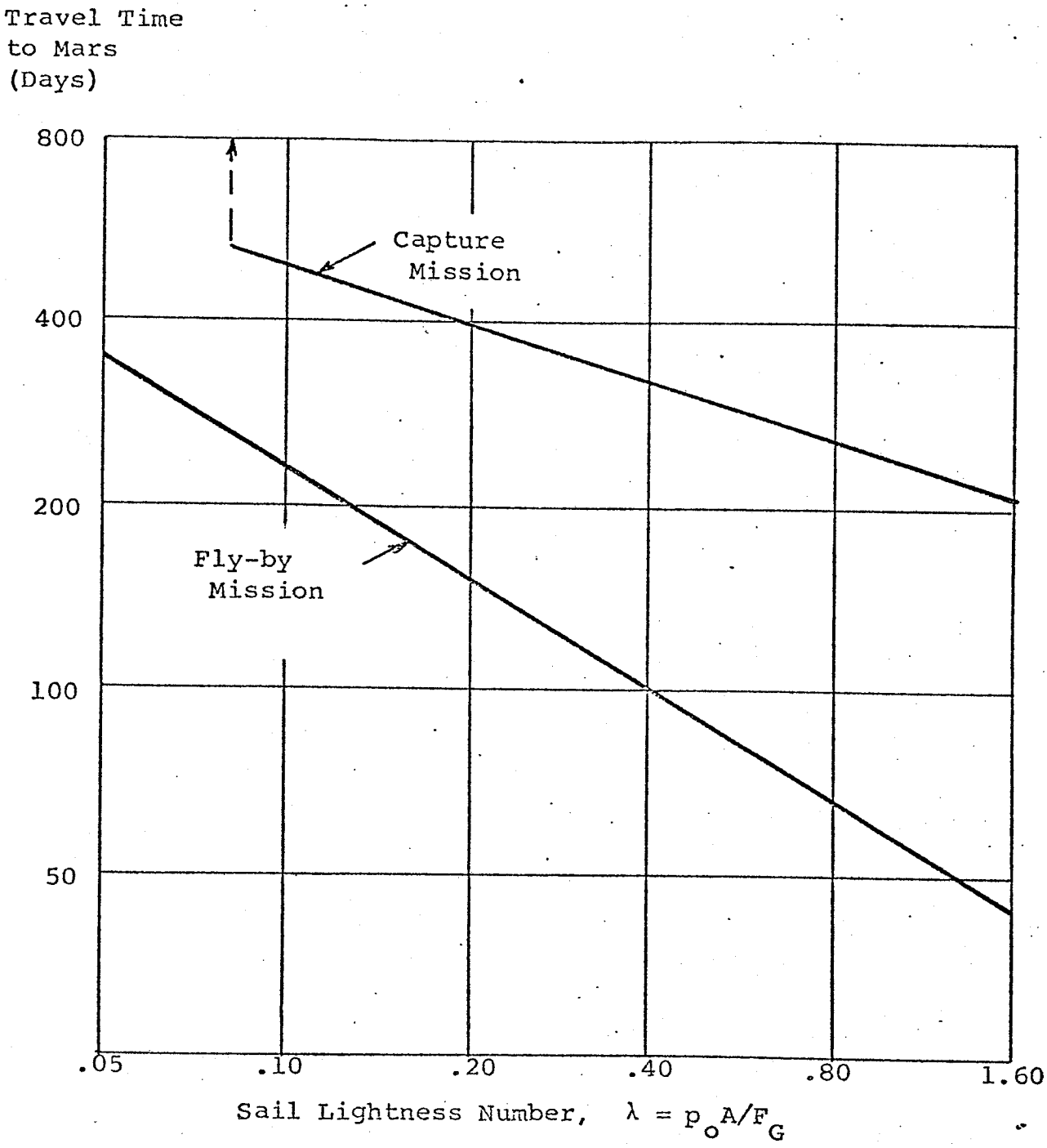

Figure 1. Travel Time to Mars for Optimum Sail Setting

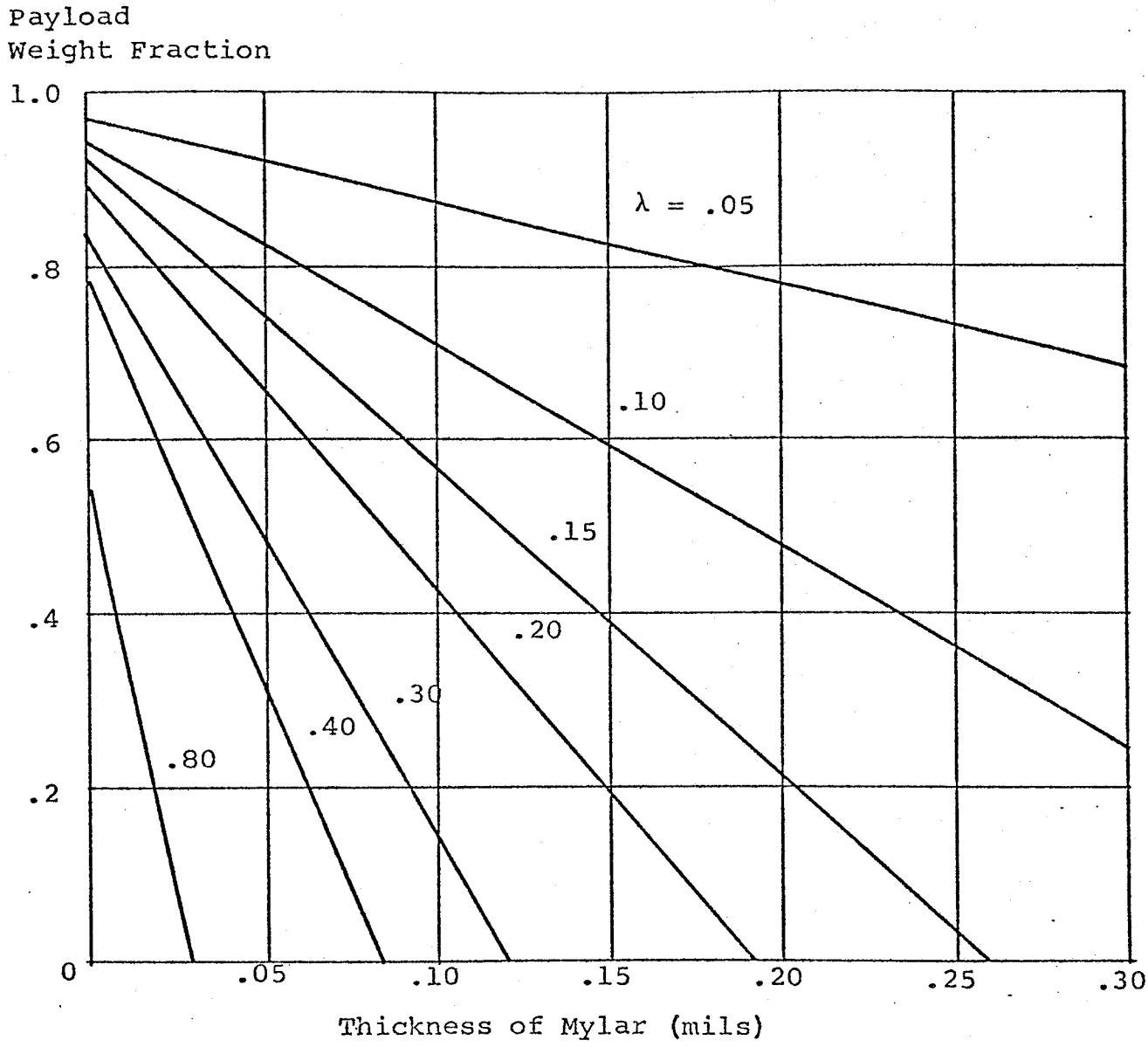

Figure 2. Payload Weight Fraction vs. Thickness of Mylar Sheet

Thickness of Aluminum = 3000 A°

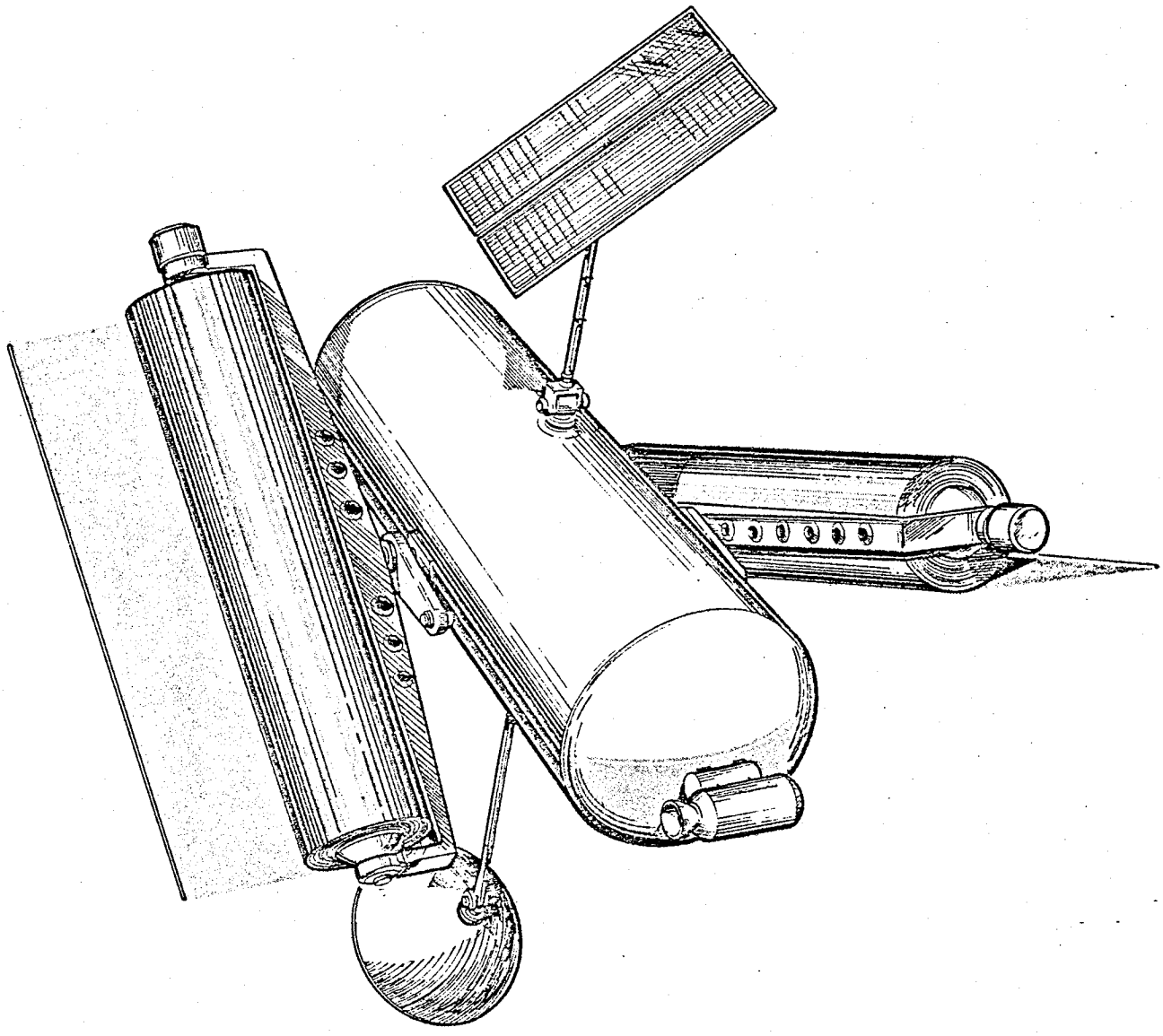

Figure 3. Sketch of Experimental Two-Blader

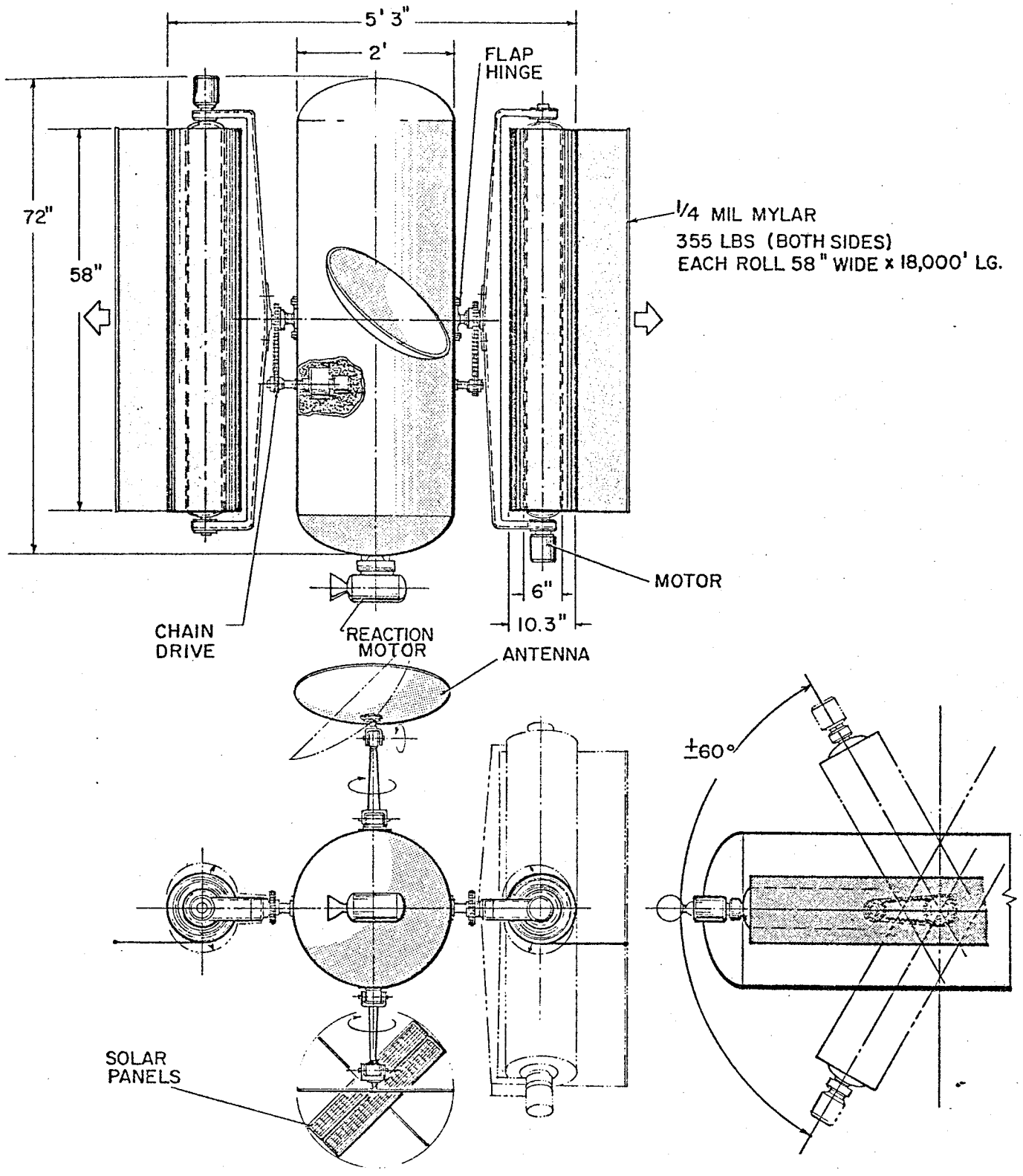

Figure 4. Three-View of Experimental Two-Blader

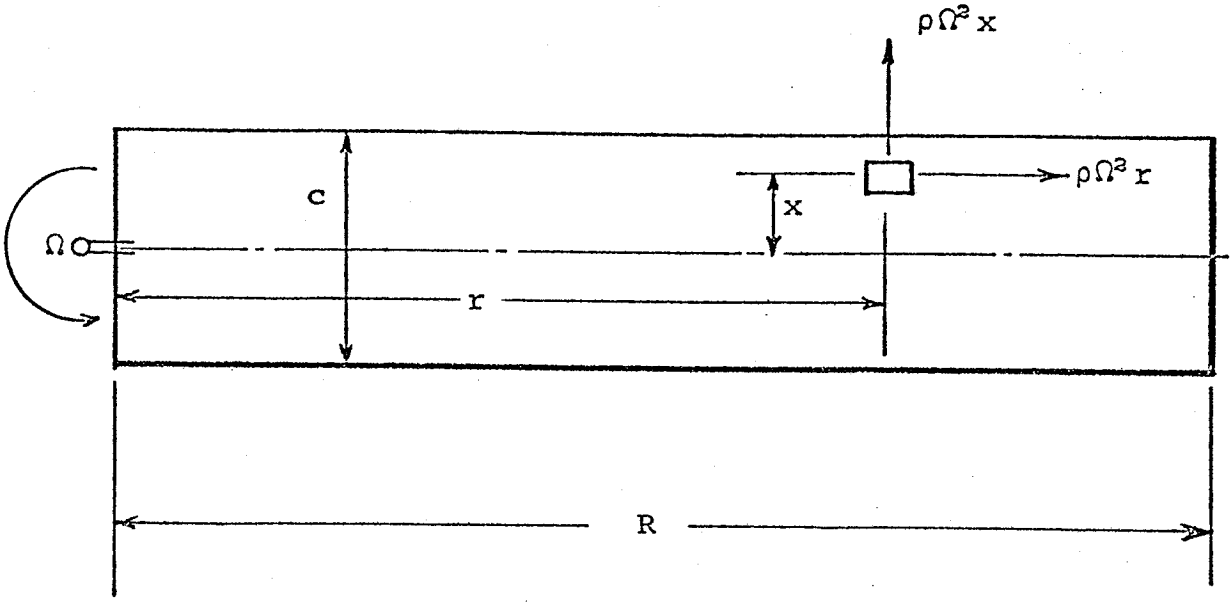

Figure 5. Centrifugal Force Field on a Blade

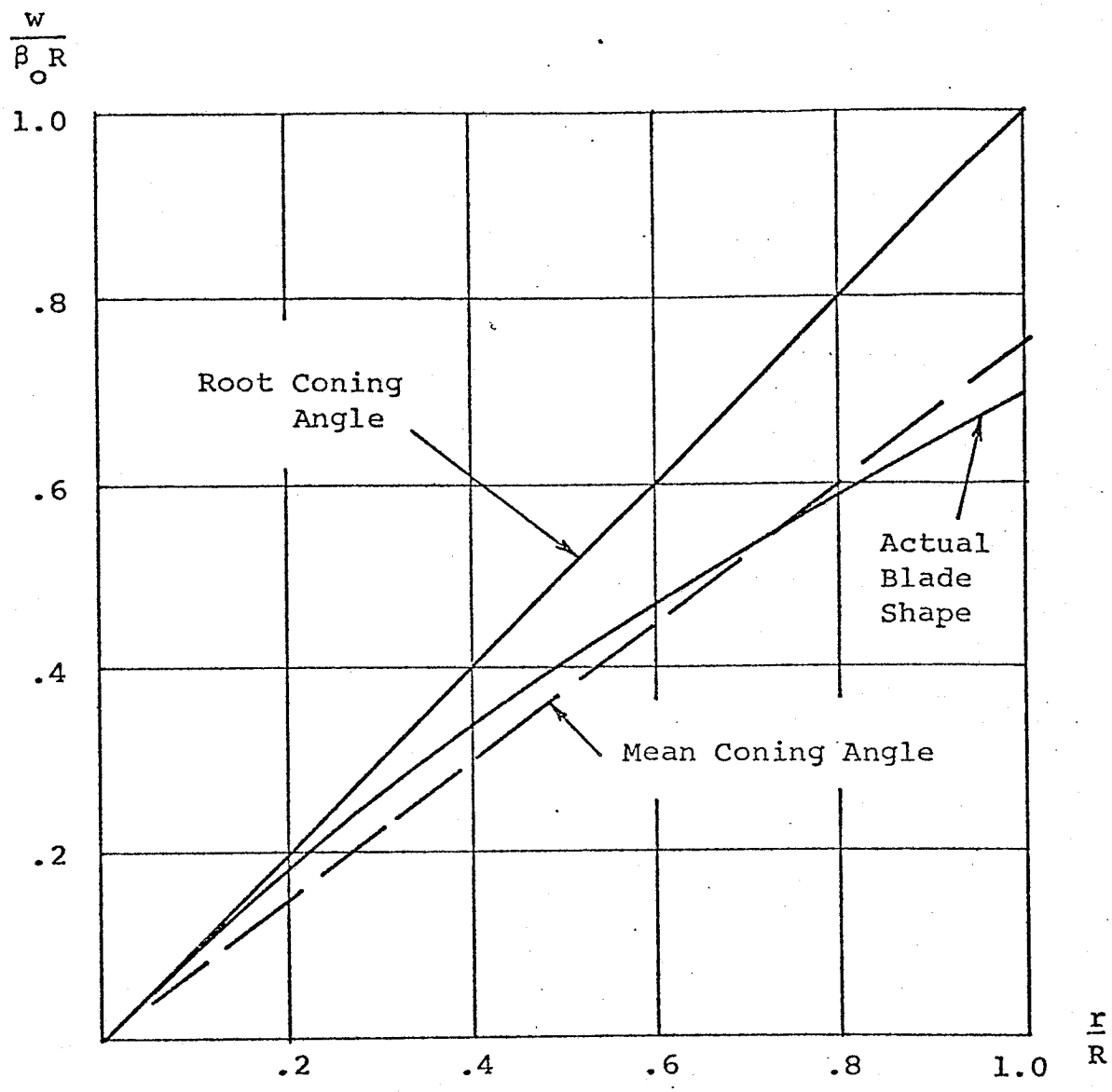

Figure 6. Vertical Blade Deflection

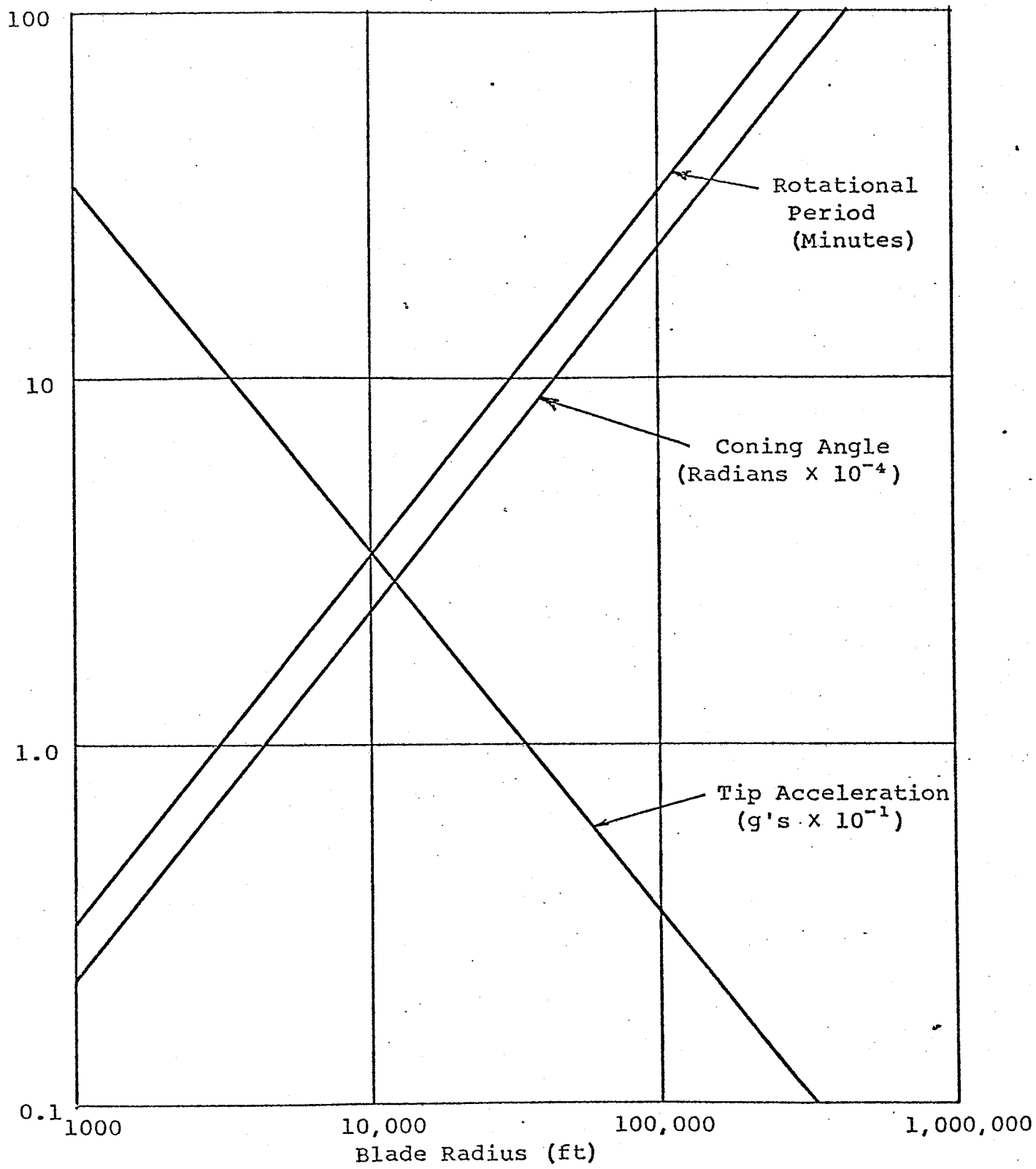

Figure 7. Operational Characteristics of ¼ mil Mylar Blade with 1000 psi Root Stress

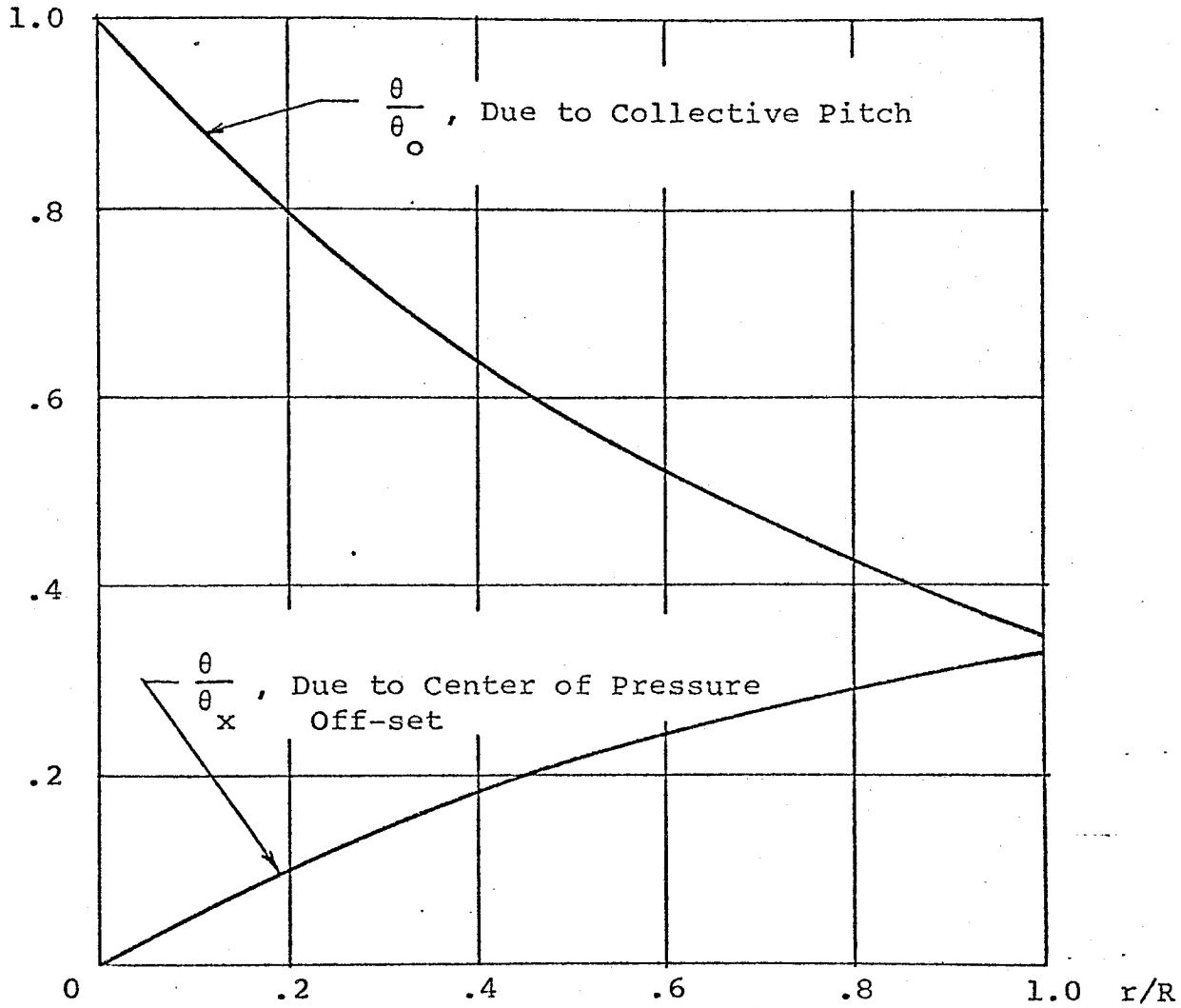

Figure 8. Blade Twist

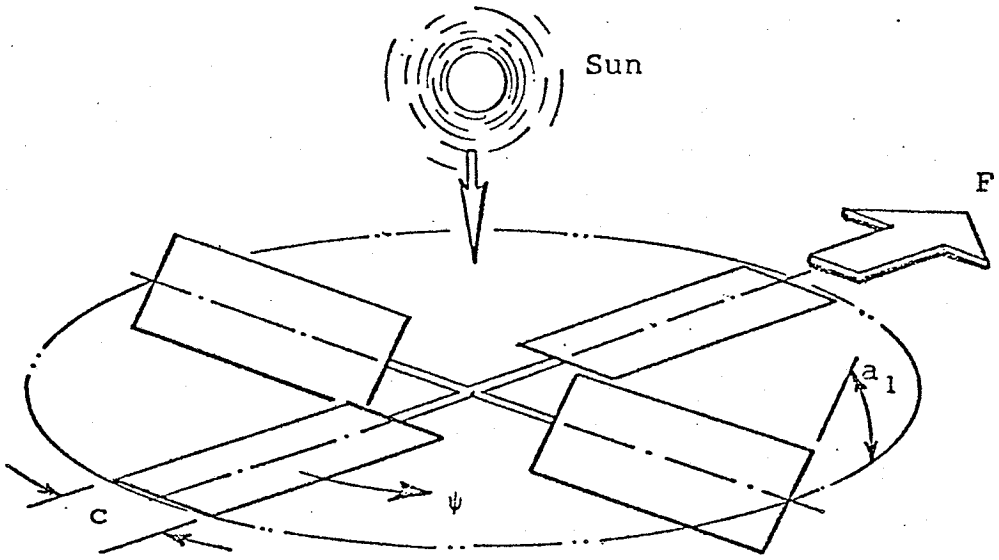

a. Lateral Force Produced by Cyclic Pitch. $\theta = a_1 \sin \psi$

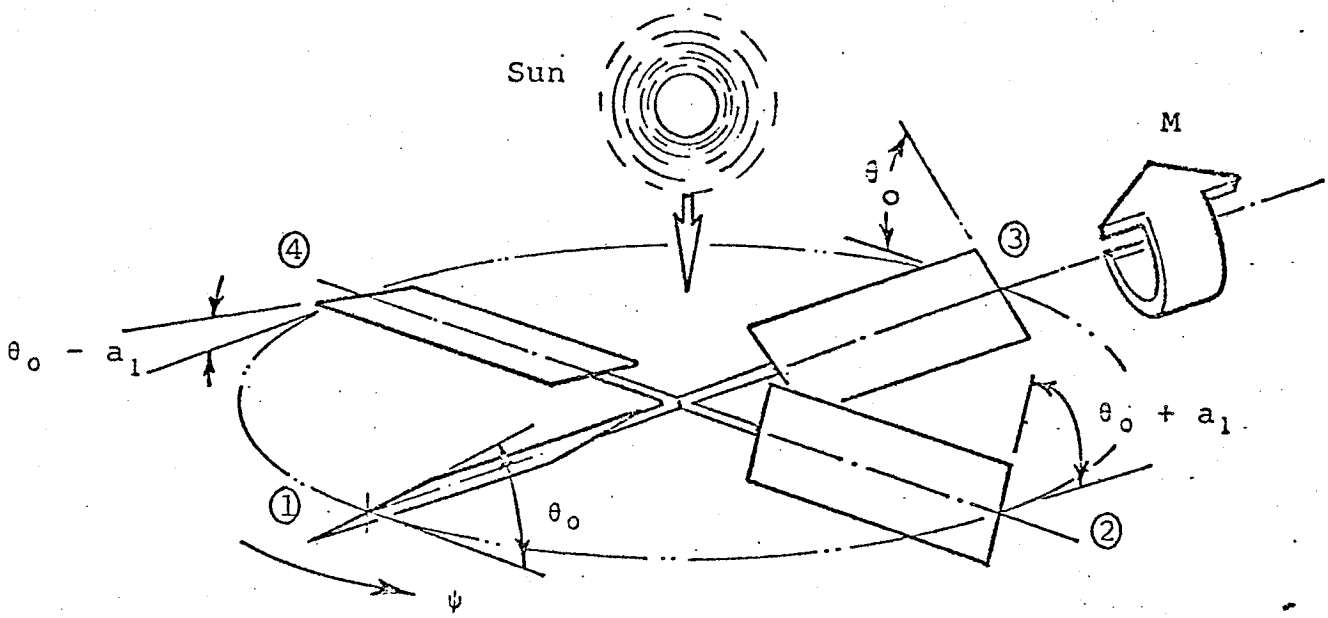

b. Rolling Moment Produced by Combined Collective and Cyclic Pitch. $\vartheta = \vartheta_c + a_1 \sin \psi$

Figure 9. Control Responses

(1) Motor Ignites
Start Spin-Up

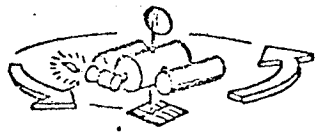

(2) Motor Stops.

Mylar Blades
Start Unrolling

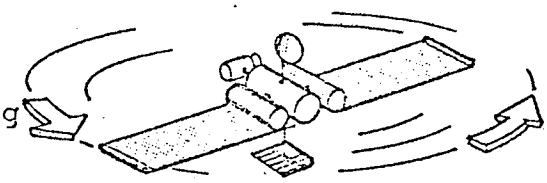

(3) Blades Unroll 326 ft Each Side
and Pitch

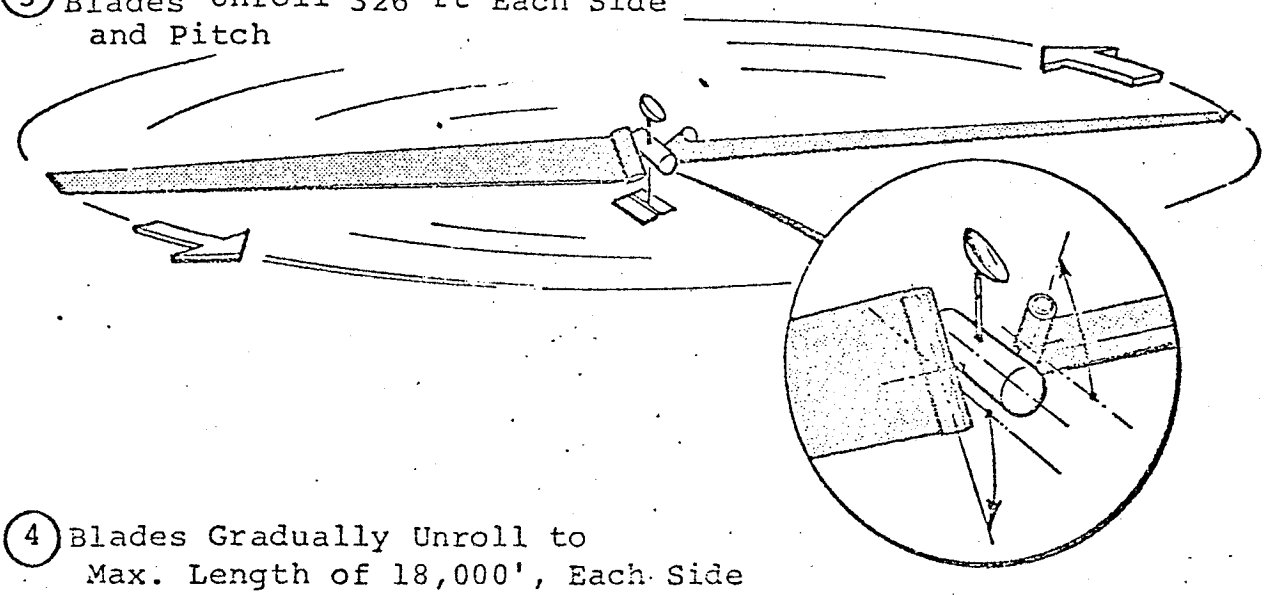

(4) Blades Gradually Unroll to
Max. Length of 18,000', Each Side

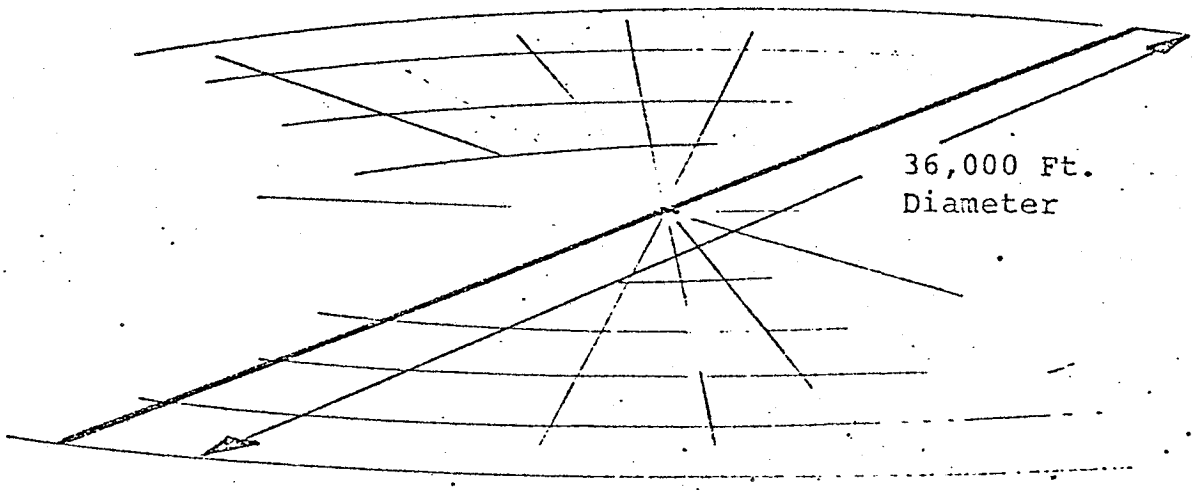

Figure 10. Deployment Sequence

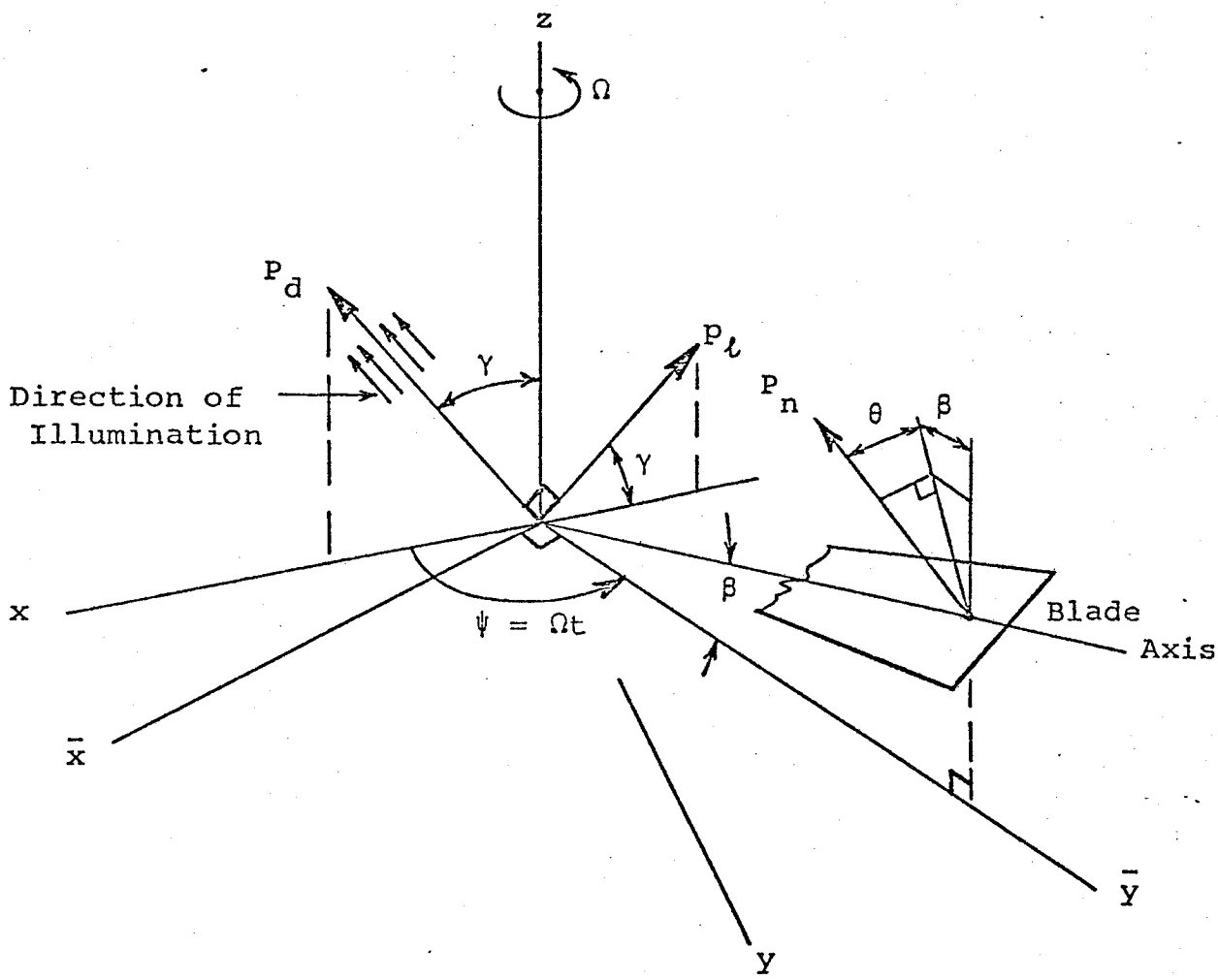

Figure 11. Coordinate Geometry For Rotating Blade

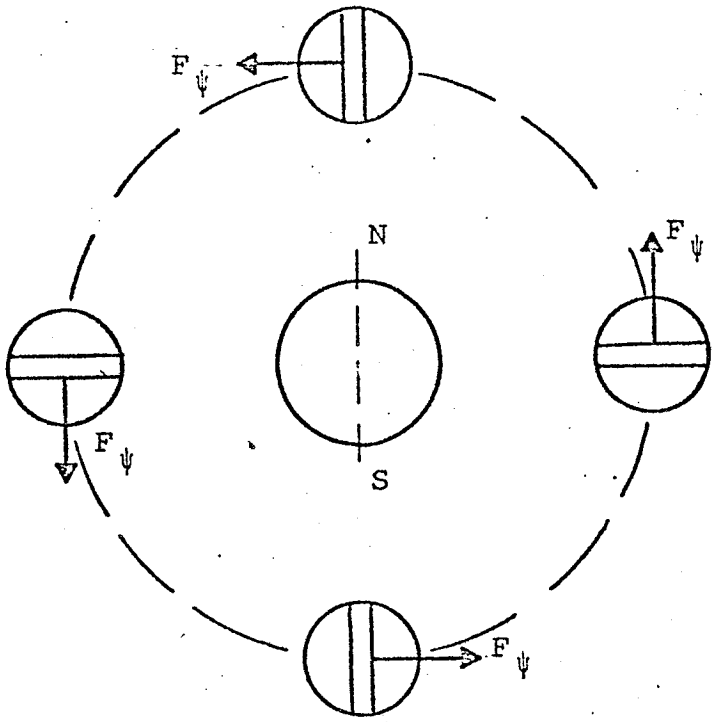

a. Polar Orbit. Use Cyclic Pitch to Produce Lateral Force

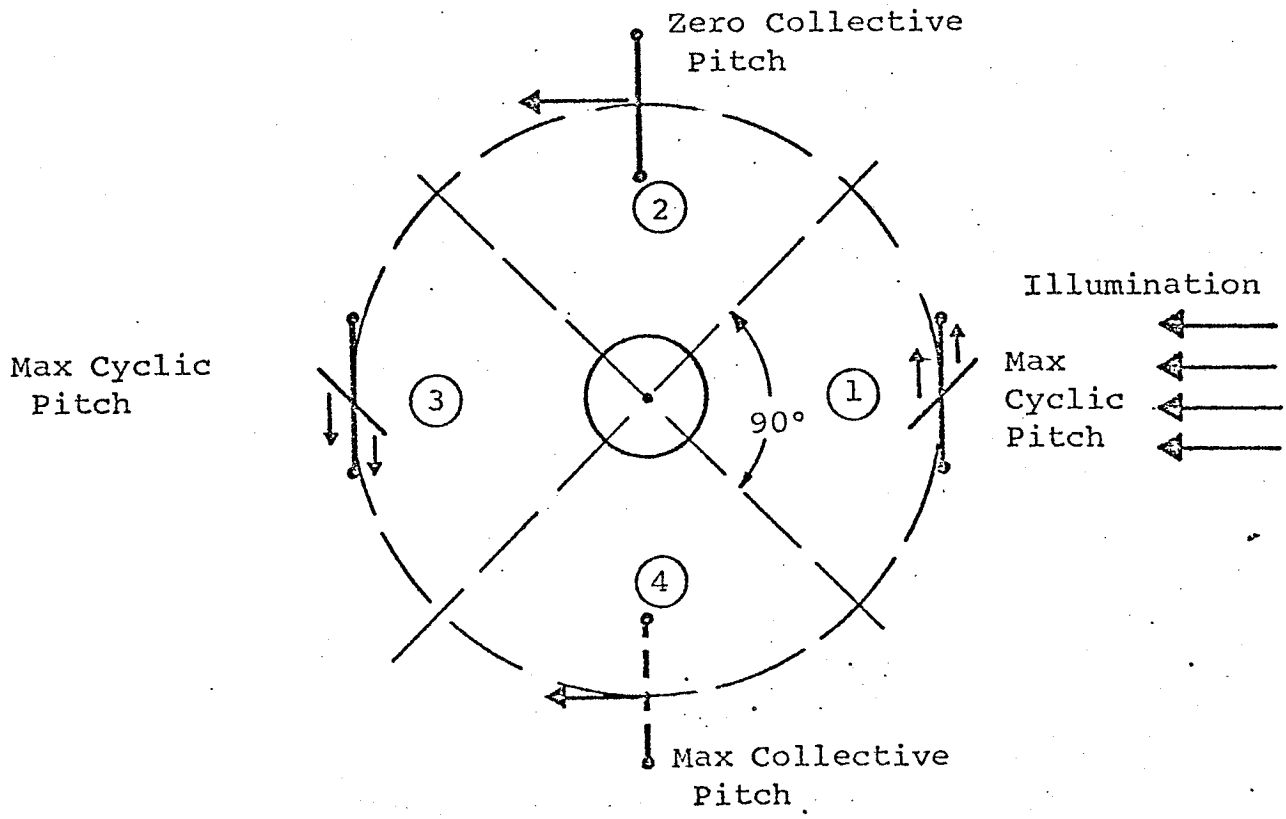

b. Equatorial Orbit. Use Both Cyclic and Collective Pitch

Figure 12. Planetary Escape Maneuvers

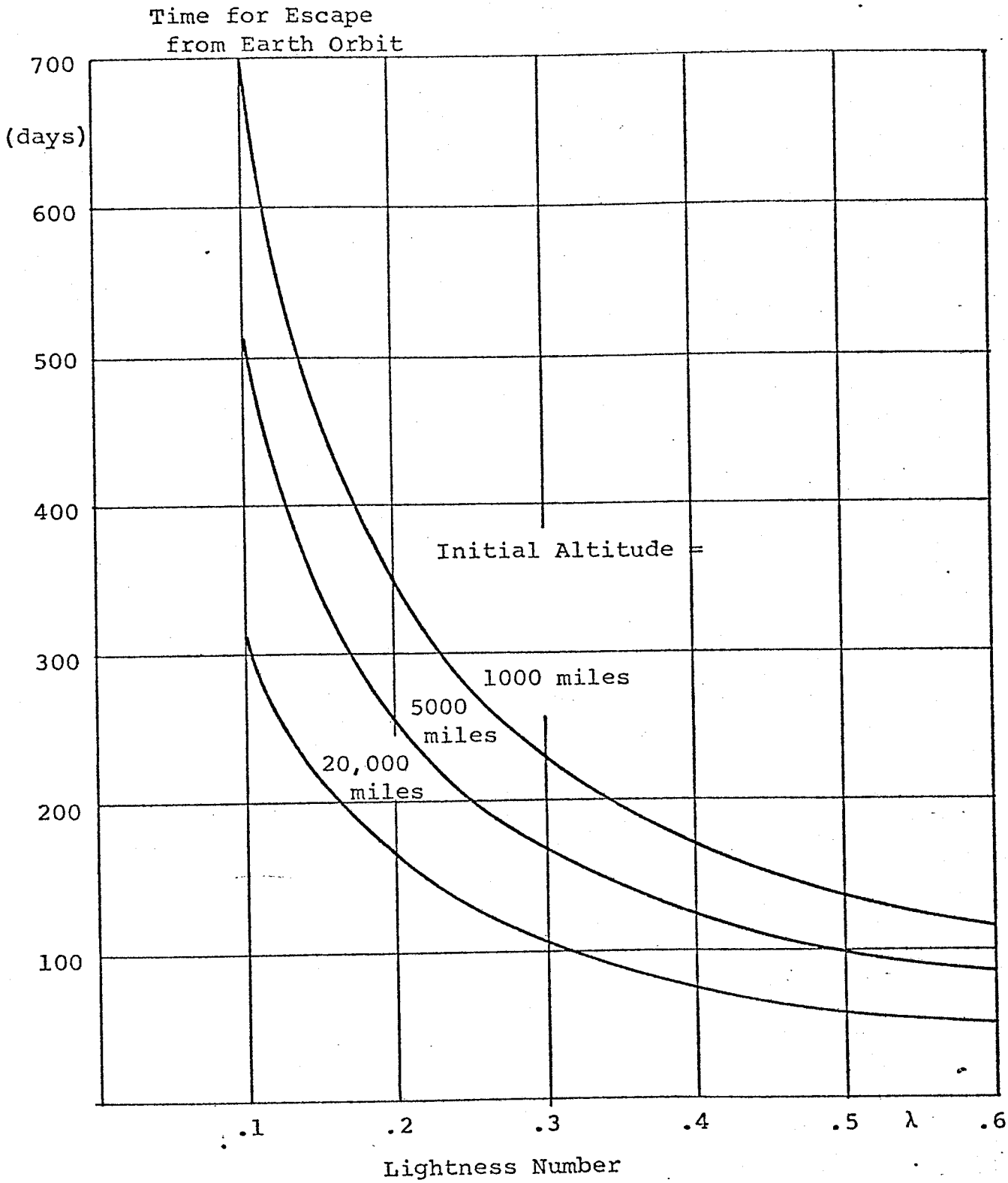

Figure 13. Time Required for Planetary Escape Maneuver from Earth Orbit

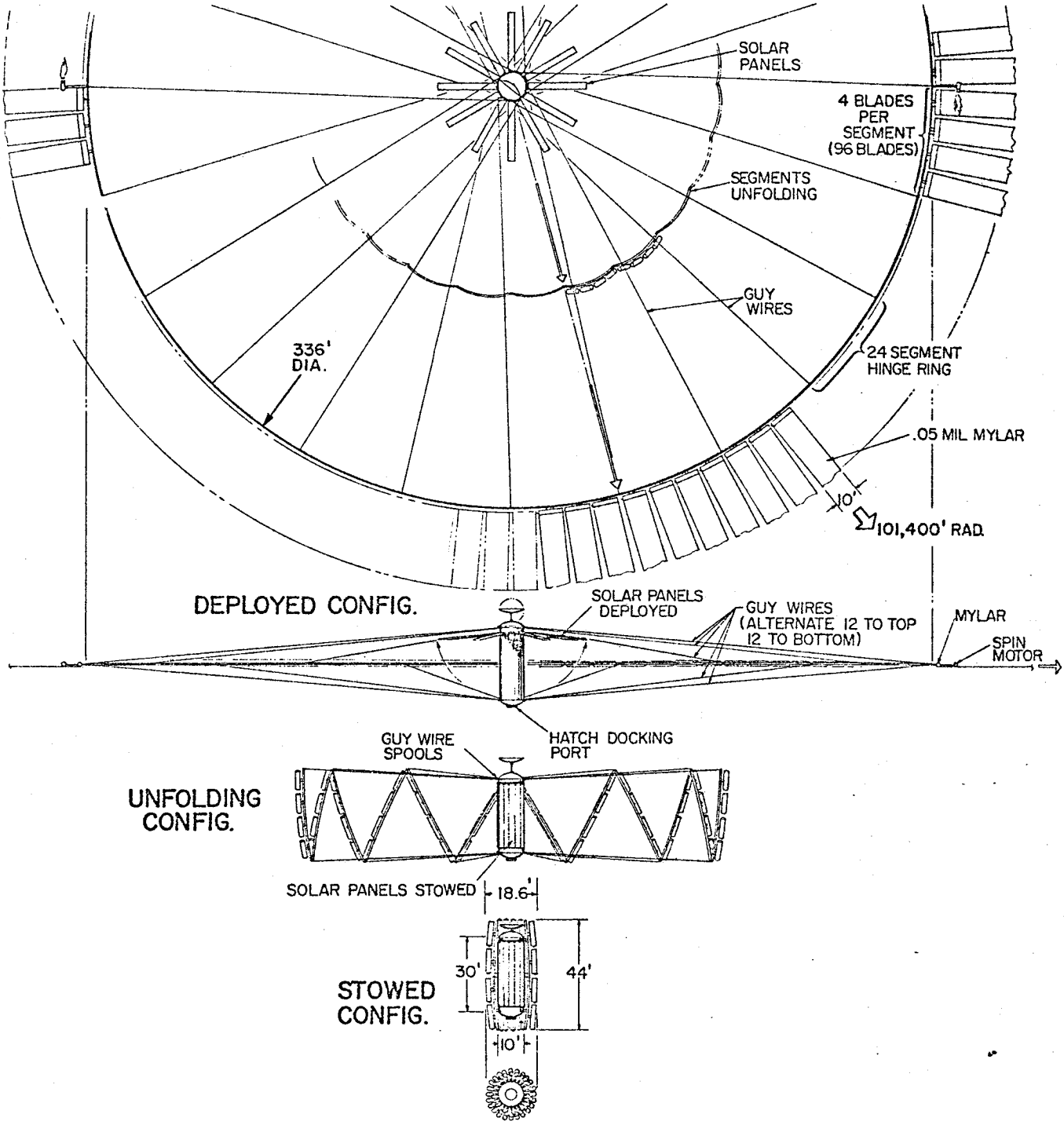

Figure 14. Pinwheel Heliogyro

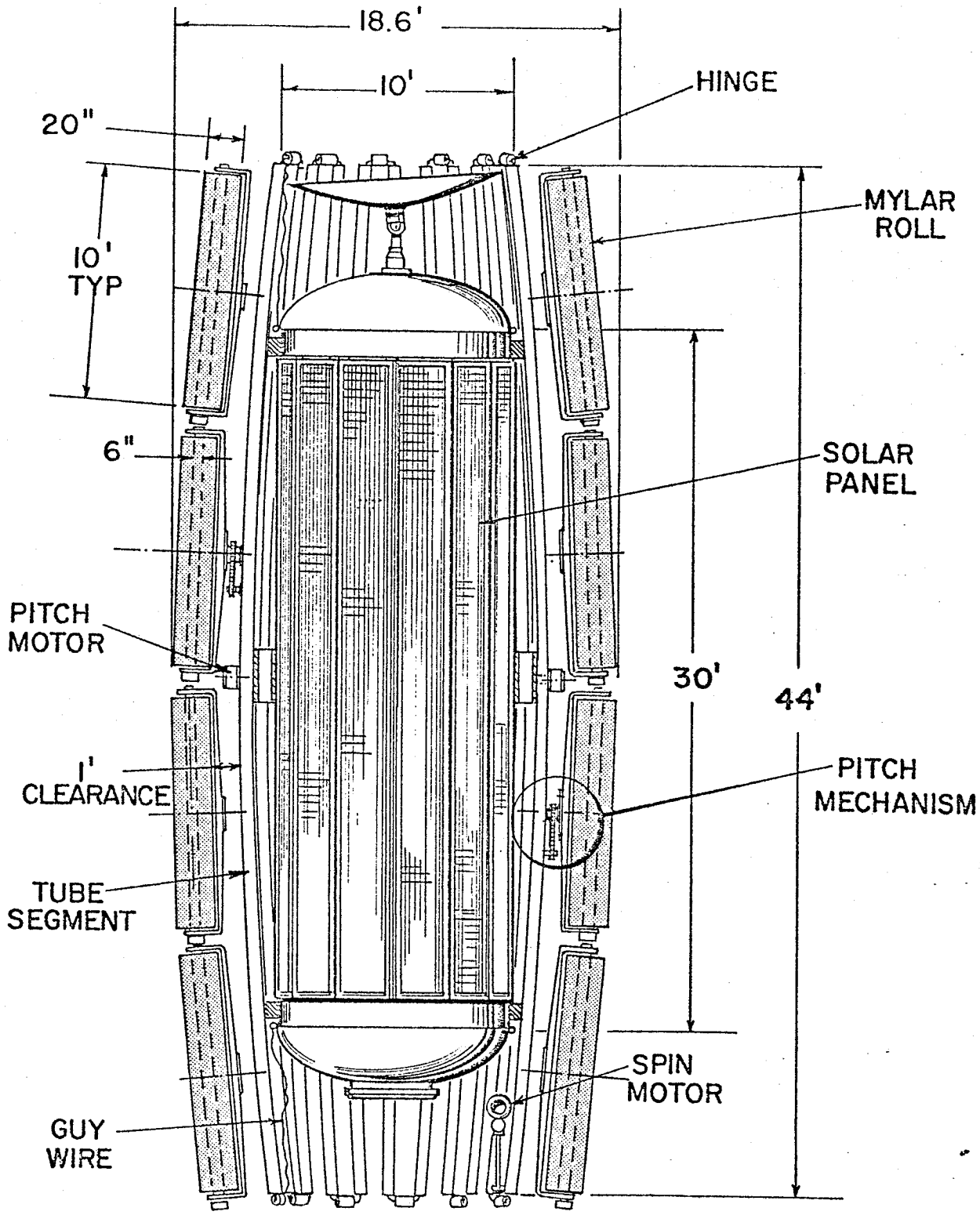

Figure 15. Pinwheel Heliogyro in Stowed Configuration

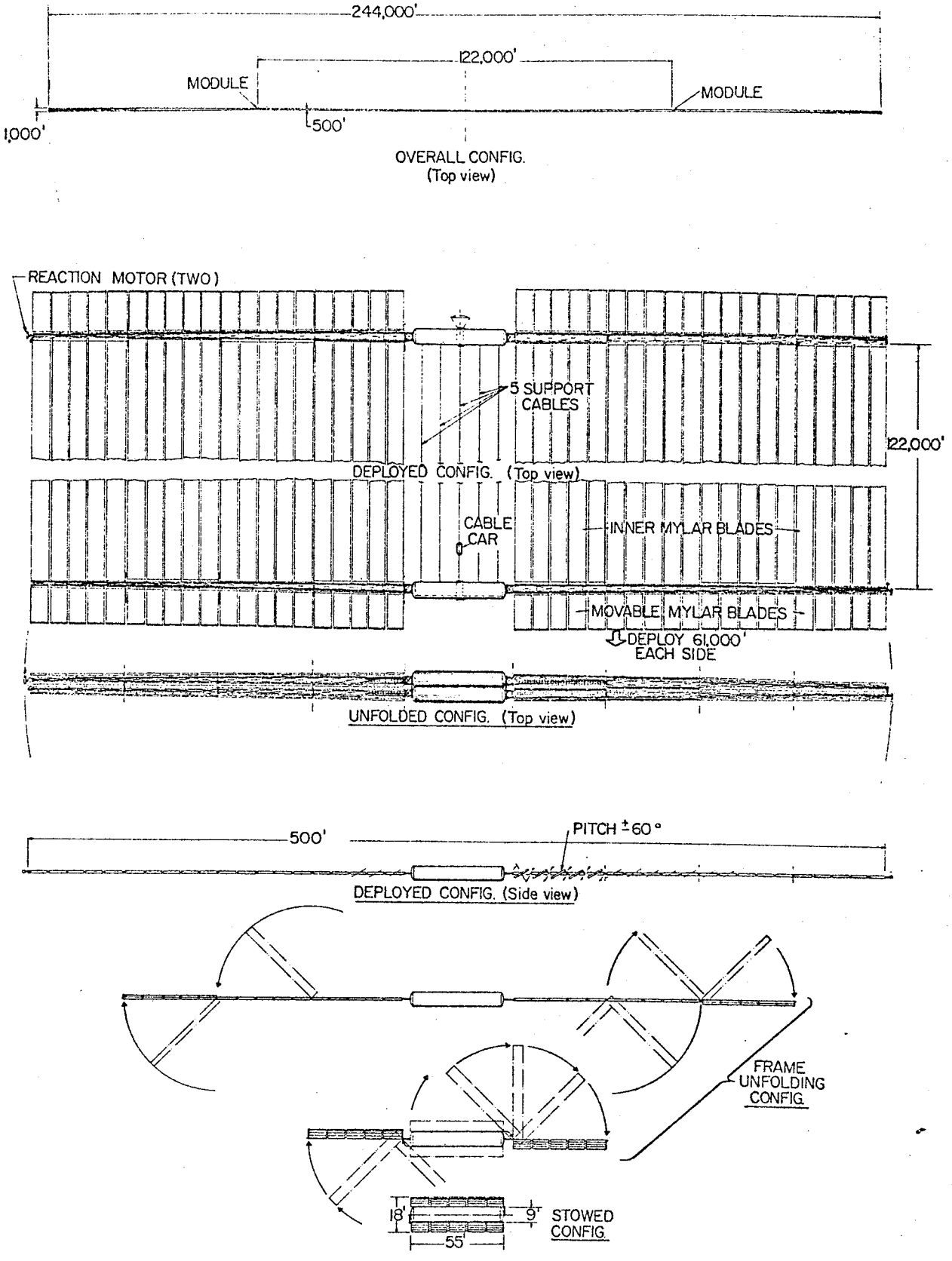

Figure 16. Parallel Blade Heliogyro

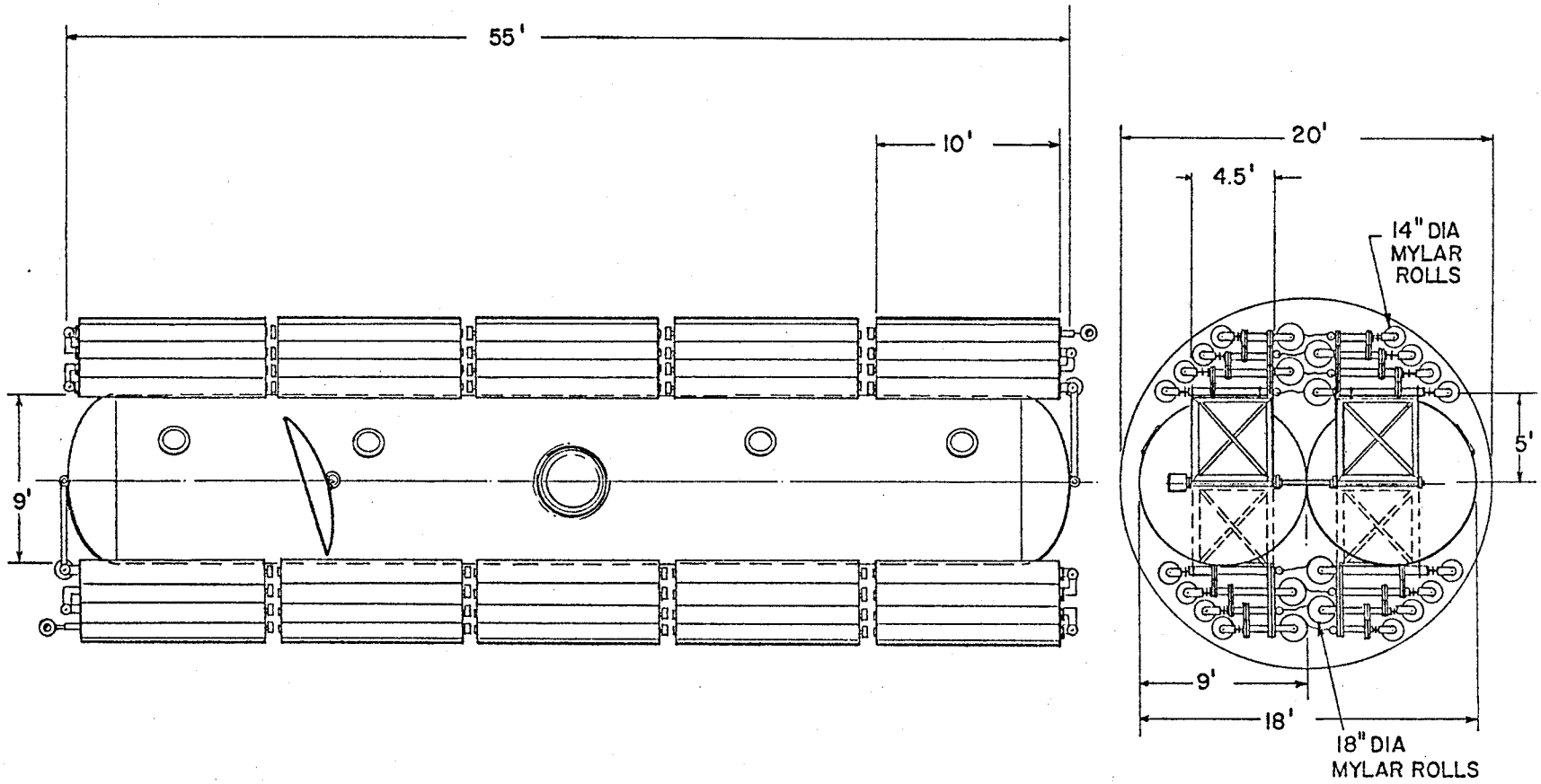

Figure 17. Parallel Blade Heliogyro in Stowed Configuration

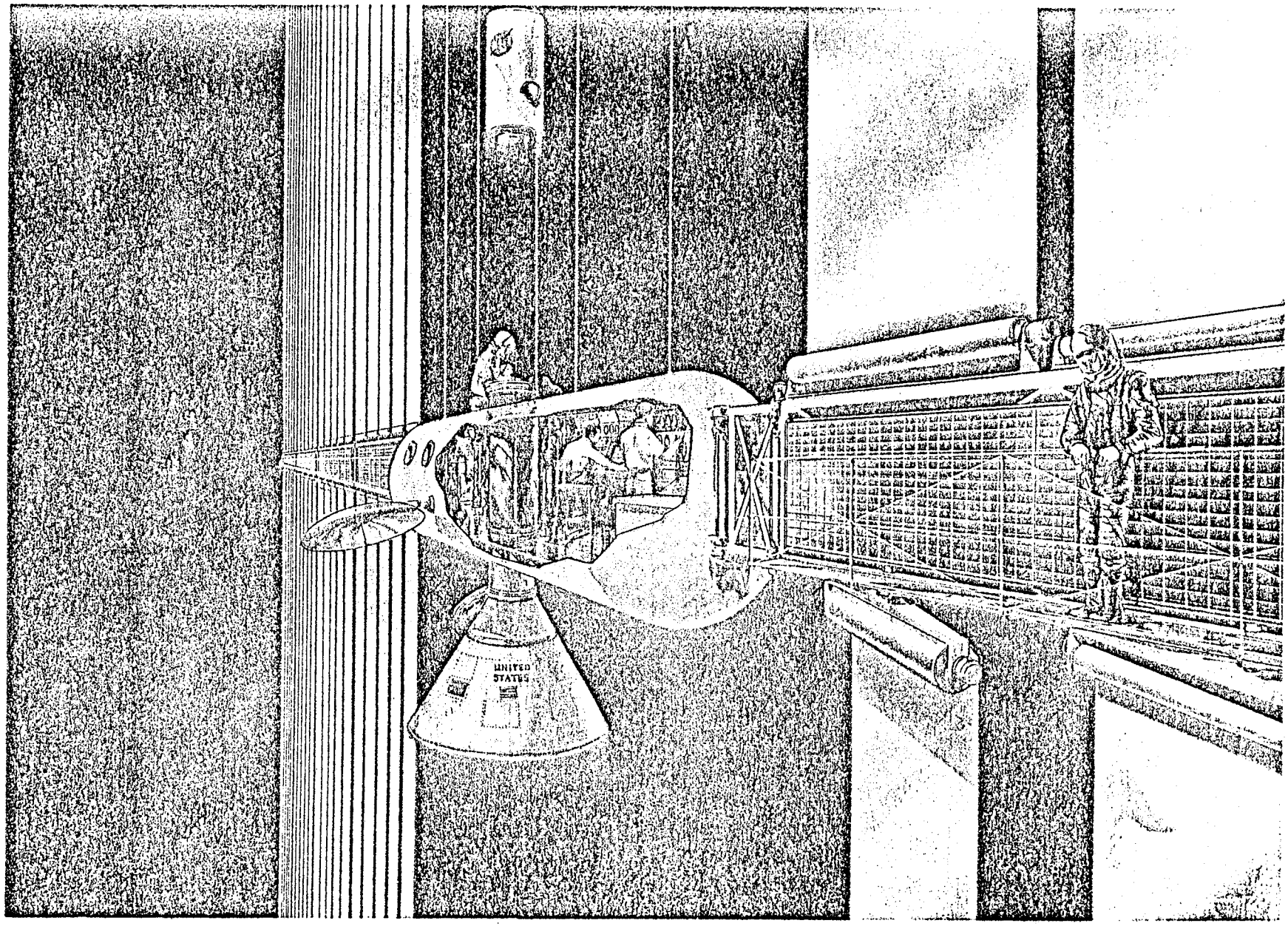

Figure 18. View of Payload Capsule

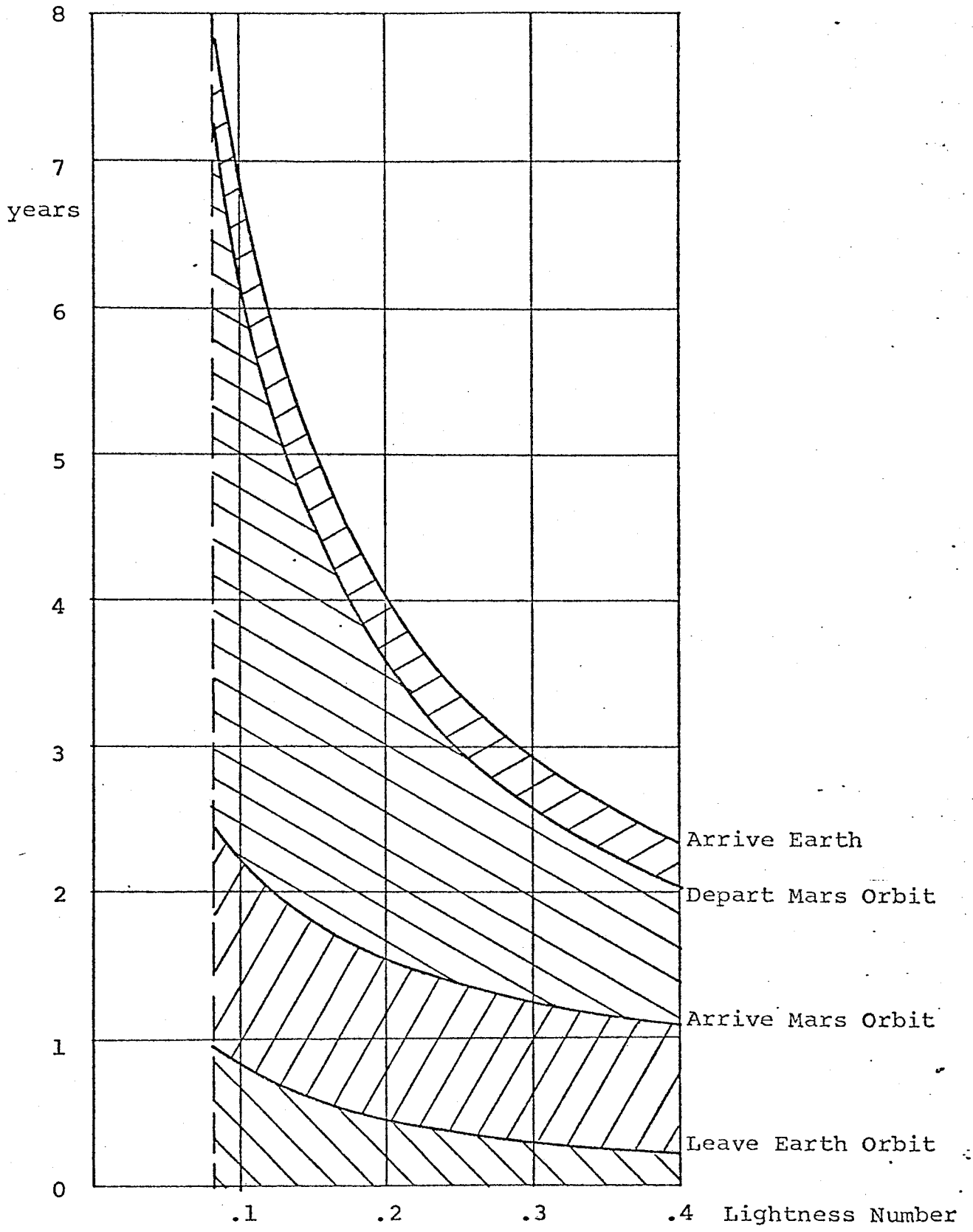

Figure 19. Elapsed Time for Mars Mission